Title

STUDY OF 16O, 20Ne, 22Ne, 28Si, AND 32S BY INELASTIC SCATTERING OF POLARIZED PROTONS

Authors

Swiniarski, R. de
Resmini, F.G.
Hendrie, D.L.
et al.

Publication Date

1973-10-01

Submitted to Nuclear Physics

STUDY OF ^{16}O, ^{20}Ne, ^{22}Ne, ^{28}Si, AND ^{32}S BY INELASTIC SCATTERING OF POLARIZED PROTONS

R. de Swiniarski, F. G. Resmini,
D. L. Hendrie and A. D. Bacher

October 1973

Prepared for the U. S. Atomic Energy Commission
under Contract W-7405-ENG-48

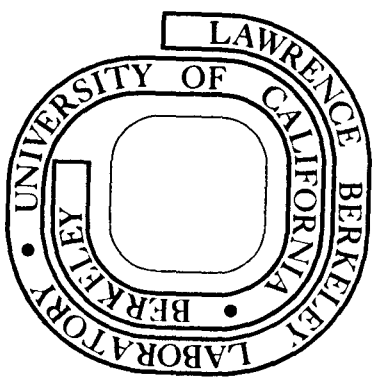

DISCLAIMER

LBL-2322

STUDY OF ^{16}O, ^{20}Ne, ^{22}Ne, ^{28}Si AND ^{32}S BY INELASTIC SCATTERING OF POLARIZED PROTONS[†]

R. de Swiniarski[††], F. G. Resmini[‡], D. L. Hendrie and A. D. Bacher[‡‡]

Lawrence Berkeley Laboratory
University of California
Berkeley, California 94720

October 1973

Abstract

Analyzing powers and cross sections have been measured for elastic and inelastic scattering of 24.5 MeV protons from ^{20}Ne and ^{22}Ne and for ^{16}O, ^{28}Si, and ^{32}S at 30.3 MeV. The experimental results were analyzed in terms of the coupled-channels formalism using the rotational model and (for ^{32}S and ^{16}O) the vibrational model. The results for ^{20}Ne, ^{22}Ne and ^{28}Si show a systematic trend of the hexadecapole deformation. Prolate shapes for ^{20}Ne and ^{22}Ne and an oblate shape for ^{28}Si are confirmed. The results for ^{32}S are almost equally well reproduced by the vibrational or rotational model. There is a slight preference for the prolate shape for this nucleus. The best fits for the analyzing power for all the nuclei were obtained by using the full Thomas form for the spin-orbit potential.

[†]Work supported under the auspices of the U. S. Atomic Energy Commission.

[††]Present address: Institut des Sciences Nucléaires de Grenoble, France.

[‡]Present address: University of Milan, Italy.

[‡‡]Present address: Physics Department, University of Indiana, Bloomington, Indiana.

1. Introduction

In the past several years, a large amount of proton elastic and inelastic analyzing power data[1-10]) have become available, arising from the increase in number and improvement in quality of polarized beam facilities. Analysis of the analyzing power data with distorted-wave Born approximation (DWBA) codes or with coupled-channels(CC) methods have been reasonably successful for collective 2^+ or 3^- levels for several nuclei in the $f_{7/2}$ shell, $g_{9/2}$ shell and s-d shell[1-8]). In order to obtain good fits in the macroscopic treatment, it was found necessary to deform the real, imaginary and spin-orbit terms in the form factor. Different ways of deforming the spin-orbit potential have been used[3]) which have led to almost equivalent results. These models were unable, however, to reproduce the large asymmmetries observed for the transitions to the first 2^+ state in ^{54}Fe and ^{52}Cr[1]). The deformed spin-orbit potential which has been previously used in the framework of the macroscopic collective model was essentially phenomenological, having a form proportional to the radial derivative of the spin-orbit term of the optical potential[3,7]). Problems have also appeared in the attempt to describe the data with microscopic models. Applications of the microscopic model to these states have usually produced poor agreement with experiment [3,6,9,11,12,13]).

More recently, H. Sherif and J. S. Blair introduced the concept of the "Full Thomas Term" in the spin-orbit potential in the DWBA collective model formalism[14]). Considerable improvements to the fits, especially at forward angles, were immediately observed[15]). Such a deformed spin-orbit term has now been included by J. Raynal in a coupled-channels program[16]). Calculations will be presented here (some of them have already been partly published

elsewhere[17]) for the analyzing powers obtained by inelastic scattering of 24.5 MeV polarized protons from the strongly excited low-lying states in ^{20}Ne, ^{22}Ne and of 30.3 MeV polarized protons for the collective states in ^{16}O, ^{28}Si and ^{32}S. Part of the purpose of this work was to test the possible improvements in the CC analysis produced by the use of the Sherif-Blair form of the spin-orbit interaction.

A second goal of the experiments was to investigate the nuclear structure of the target nuclei. Recent coupled-channels calculations[18]) have shown the existence of a large Y_4 deformation in the K = 0 band in ^{20}Ne and suggest the possible existence of such hexadecapole deformation in other s-d shell nuclei. Moreover since recent (α,α')[19]) or (^{3}He, ^{3}He')[20]) experiments have yielded large differences in the evaluation of the Y_4 deformation of s-d shell nuclei, polarization experiments can provide additional information for a more precise determination of the deformations. The rotational model provides a reasonably accurate description of the low-lying levels in some s-d shell nuclei, for instance ^{20}Ne and ^{28}Si, but the situation is less clear for ^{32}S. We had originally hoped that analyzing power measurements would allow a clear distinction between rotational and vibrational models for the low-lying states of ^{32}S, but this was not found to be so.

Since cross-section data for inelastic proton scattering on ^{20}Ne at 24.5 MeV[21]) and on ^{28}Si[22]) and ^{16}O[23]) at 30.3 MeV were already available, emphasis was concentrated on the measurement of the analyzing power. Cross sections for ^{22}Ne(p,p') and ^{32}S(p,p') were obtained simultaneously with the polarization data and are therefore somewhat less precise.

After a brief description of the experimental method in section 2, the analyzing power data for ^{16}O, ^{20}Ne, ^{22}Ne, ^{28}Si and ^{32}S are presented in section 3. The discussion of the optical model analysis for the different nuclei is made in section 4, while section 5 discusses the coupled-channels calculations using various spin-orbit distortions and deformations. A short summary of the conclusions is given in section 6.

2. Experimental Method

The experiments were performed using the Berkeley 88" cyclotron and polarized ion source[24]). The source is of the atomic beam type and uses an adiabatic RF transition and strong field ionizer. The polarized ion beam is injected axially[25]) into the center of the cyclotron and deflected into a proper orbit by a gridded electrostatic mirror. During these experiments, up to 60 nA of beam were delivered onto the target with an average polarization of about 75%. The beam polarization was monitored continuously with a standard ^{12}C polarimeter[26]), which was subsequently calibrated by accurate p-^{4}He polarization measurements at the same energy[27]). The beam intensity was continuously monitored with a pair of Si(Li) detectors placed symmetrically at 45 degrees with respect to the beam direction and was checked periodically with a Faraday cup. The thick polarimeter target precluded the continuous use of a Faraday cup.

The data were taken with eight 5 mm thick Si(Li) detectors cooled by thermoelectric devices to about -25°C. In order to measure asymmetries, the counters were arranged in symmetric pairs to the left and right of the beam direction. In addition, the beam polarization was manually reversed at the source by inverting the magnetic field of the ionizer half way through each data taking run. This redundancy of asymmetry measurements allowed us to eliminate many sources of systematic error, such as those due to uncertainties in counter apertures, slight misalignments of the beam, and differential counting rate effects in the detectors and in the polarimeter.

The ^{28}Si target was a slightly enriched ($\geq$ 95%) self-supporting foil of $\sim$ 400 $\mu g/cm^2$ thickness. ^{32}S and ^{16}O data were taken simultaneously using a

SO_2 gas target. The neon gas targets were filled with isotopes enriched to $> 99.9\%$ for ^{20}Ne and $\geq 95\%$ for ^{22}Ne. All gas targets were operated at about 20 cm.Hg pressure, which was measured together with the temperature before and after each run. The overall energy resolution was about 180 keV for the gas target data and about 150 keV for the ^{28}Si data, the latter being mostly due to the energy spread of the incident beam. Except for the 3^-, 1^- doublet in ^{20}Ne at 5.7 MeV and the 2^+, 4^+ doublet in ^{32}S at 4.4 MeV, all strongly low-lying excited states of the s-d shell nuclei were clearly separated.

3. Experimental Results

The measured analyzing powers for the low-lying excited states in ^{20}Ne and ^{22}Ne are shown in figs. 1 and 2; the data were taken with an incident beam energy of 24.5 MeV. These two figures exhibit the similarities that exist for the lowest 0^+ and 2^+ states in ^{20}Ne and ^{22}Ne. Moreover, cross sections to the 0^+ and 2^+ states in ^{20}Ne and ^{22}Ne, to be seen in later figures, are also very similar; this being true also at higher energy[28]). This is not the case for the 4^+ states in ^{20}Ne and ^{22}Ne, where large differences exist between the two analyzing powers as well as between the two cross sections. It is also worthwhile to point out the large difference between the analyzing power for the first and second 2^+ states in ^{22}Ne (fig. 2). Such a large difference has already been observed in the $f_{7/2}$ shell[9]) and suggests the need for a microscopic interpretation. Figure 3 shows the analyzing power for the K = 0 rotational band in ^{28}Si together with the strongly excited 0^+, 2^+ and 3^- states in ^{32}S while fig. 4 presents the analyzing power for several states in ^{16}O. The data presented in figs. 3 and 4 were taken at an energy of 30.3 MeV. Here also a striking difference can be seen between the 2^+ curves in fig. 3. The first bump on the ^{32}S curve at 50° is much lower than in the corresponding curve for ^{28}Si and resembles the shape of the analyzing power taken at 20.3 MeV for ^{24}Mg[3]).

The analyzing power presented in figs. 1 to 4 are normalized to 100% beam polarization and are defined as follows (in first approximation)

$$A = \frac{1}{P_B} \frac{r-1}{r+1}$$

with $$r = \left(\frac{N_{+L} \cdot N_{-R}}{N_{+R} \cdot N_{-L}}\right)^{1/2}$$

where N_{+L}, N_{-L} and N_{+R} and N_{-R} are the number of counts in a given peak to the left or to the right of the beam direction (for the same angle) with spin-up and spin-down respectively, while P_B is the polarization of the beam.

The analyzing powers for the 0^+(g.s) and 2^+ state in ^{28}Si and for the 0^+(g.s) in ^{16}O are in good agreement with other recent data[4,6]).

The error bars shown on the figures reflect only statistical errors unless the peaks were difficult to resolve, in which case the errors were increased appropriately. Most of the integrated counts were obtained from the spectra with a peak fitting program[29]) and were checked for internal consistency.

4. Analysis

4.1. OPTICAL MODEL PARAMETERS FOR ^{20}Ne AND ^{22}Ne

Since ^{20}Ne and ^{22}Ne are strongly deformed, only preliminary optical model parameters needed for the CC calculation can be obtained from a optical model search. In their analysis of α-scattering in the rare earth region, Hendrie et al.[30]) obtained good fits for the rotational band cross sections by first deriving optical model parameters from a nearly spherical nucleus and then using these parameters in a coupled-channels calculation for the deformed nuclei. Such an attempt has been made by trying to use the optical model parameters obtained from an analysis of the elastic cross section and polarization data of ^{16}O taken from the literature[31]) but this has failed completely to describe the excited states of ^{20}Ne. The method which was finally chosen, at least for ^{20}Ne and ^{22}Ne, was to get a starting set of optical model parameters from a multi-parameter search using the elastic scattering data and then to adjust the parameters so as to preserve the fits to the elastic scattering in the coupled-channels calculations. In the case of ^{20}Ne and ^{22}Ne, it was found that only slight adjustments of W_D, a_I and V_o, a_o were needed.

Table 1 lists the best-fit parameters obtained from a search on all parameters. The corresponding fits to the elastic cross sections and polarizations are shown in fig. 5. Most of the optical model calculations were carried out with the code MAGALI[32]). The absolute normalization of the data was included in the search and only statistical errors for cross sections and polarizations were taken into account. Corrections arising from the finite angular acceptance of the detectors were included in the search. It is interesting to point out the common result that r_{LS}, the radius of the spin-orbit potential, is smaller than the real central radius by about 20%, while the imaginary radius r_I comes

out larger ($\geqslant 20\%$) than this central radius. Moreover, parameter sets for ^{20}Ne and ^{22}Ne are quite similar, both sets having a very small spin-orbit diffuseness.

4.2. OPTICAL MODEL PARAMETERS FOR ^{16}O, ^{28}Si AND ^{32}S

The data for these nuclei have been taken at an energy of 30.3 MeV with the same experimental equipment described in Section 2. Since only analyzing powers for ^{16}O and ^{28}Si were obtained during these experiments, calculations were carried out using the elastic cross sections of ref. 31 for ^{16}O and of ref. 22 for ^{28}Si. On the other hand, cross sections for the 0^+, 2^+ and 3^- states in ^{32}S were obtained simultaneously with the analyzing power data. Very good fits were obtained for these three nuclei as shown in figs. 6 and 7. The corresponding parameters are presented in Table 1. The fit to the ^{32}S elastic analyzing power could be obtained only by reducing, by a large amount, the spin-orbit radius r_{so}. All searches done on the ^{32}S elastic data favor this small spin-orbit radius and a comparably large spin-orbit diffuseness.

Probably because ^{28}Si and ^{32}S are less deformed nuclei than ^{20}Ne, the parameters obtained by the optical model search gave quite good fits in the coupled-channels calculations without having to be modified.

It is possible to deduce from Table 1 some systematic trends for the optical model parameters in going from ^{20}Ne to ^{32}S. We find a smaller radius (average around 1.07 fm) and a larger diffuseness (average value around 0.73 fm)

than have previously been ascribed to the real potential. If the imaginary radius remains constant around 1.33 fm, the tendency of the spin-orbit potential is to have both its radius and diffuseness smaller than those of the real central well (except for the special case of ^{32}S). These conclusions have already been given in a recent review paper on this subject[33]) for heavier nuclei, but it is interesting that they are also valid for light nuclei. Some searches were also made including volume absorption terms, but no significant improvement was seen.

5. Coupled Channels Calculations

The spectrum of excited states in most nuclei in the 2s-1d shell exhibits a rotational character[34]) indicative of a permanent deformation. The large static quadrupole moments for the first excited states[35]) and the results of Hartree-Fock and Hartree-Fock-Bogoliubov type calculations[36]) also characterize the s-d shell as a region of permanent ground state deformation. Some of these calculations suggest that some nuclei in this region should also have a ground state hexadecapole deformation, which changes both size and sign through the shell, together with the quadrupole deformation[37-39]). Data from the inelastic scattering of protons[18]) and alpha particles[19]) on ^{20}Ne, analyzed in the coupled-channels formalism, have shown that a large hexadecapole deformation (β_4) was needed to reporduce both the shape and the magnitude of the cross sections leading to the lowest 2^+, 4^+ and 6^+ states in ^{20}Ne.

Similar analyses[18,19]) of other inelastic scattering data in the s-d shell has shown that the Y_2 and Y_4 moments vary considerably throughout this region. Nevertheless, considerable differences in the value of the hexadecapole deformation β_4, especially in the case of ^{20}Ne, were obtained depending upon the type of particles used in the scattering experiments[18-20,40,41]). The additional information provided by analyzing power measurements has been shown to be helpful in resolving such ambiguities[17,42]).

The strong couplings between states of the ground state rotational band requires the use of the coupled-channels (CC) reaction formalism in order to treat adequately the multiple paths of excitation to the excited states[43]). In this formalism, the intrinsic deformation of the members of the

K = 0 rotational band is parametrized according to the following definition of the nuclear radius

$$R(\theta) = R_o[1 + \beta_2 Y_{20}(\theta) + \beta_4 Y_{40}(\theta)] \quad .$$

The interaction potential arises from the deformation of the real and imaginary central potentials, the spin-orbit potential, and the Coulomb potential. The various multiple-excitation paths between the coupled states are explicitly included, assuming pure rotational matrix elements between them. All expansions are carried to convergence, so that the only approximations are in the nuclear model and those inherent in the CC formalism[43].

5.1. COUPLED-CHANNELS CALCULATIONS: ^{20}Ne AND ^{22}Ne

Previously reported CC calculations[17,18] on ^{20}Ne were made with the Oxford coupled-channel code[44]. This program uses a simplified symmetrized form (phenomenological) of the deformed spin-orbit potential[3], in which the deformation appears only in the radial term of the spin-orbit form factor. These CC calculations essentially fail to reproduce even the shape of the observed analyzing powers for the 2^+ and 4^+ states in ^{20}Ne. Since the cross-sections leading to these states are so well reproduced[18], it is reasonable to suspect the difficulty arises from the form of the deformed spin-orbit potential which this program uses. Recent calculations have shown that the fits to analyzing power data for less strongly coupled nuclei can be significantly improved when the full Thomas term of Sherif and Blair for the deformed spin-orbit potential is used[14,15]. This full Thomas term has been introduced

by J. Raynal in a coupled-channels program using a sequential iteration technique to handle the additional complexity of this potential[16]) (Program ECIS 71). The results of such calculations for ^{20}Ne are also shown in fig. 8. As can be seen from this figure, the CC calculations reproduce well the measured analyzing power when the full Thomas term is used (curve 1, fig. 8). Curve 2 with $\beta_4 = 0.0$ shows the pronounced sensitivity of the analyzing power of the 2^+ and 4^+ states to the Y_4 deformation. The last curve (curve 3) on this figure presents the results of CC calculations using the simplified symmetrized form of the deformed spin-orbit potential, clearly showing the poor quality of the resulting fit. The corresponding CC calculations for the 0^+, 2^+ and 4^+ cross sections in ^{20}Ne are presented in fig. 9 where the sensitivity to the β_4 deformation can be seen even for the 0^+ (g.s.). On the other hand, cross sections are rather insensitive to the detailed form of the spin-orbit potential and therefore only calculations using the full Thomas term are presented in fig. 9. While the value obtained for β_2 for ^{20}Ne is in relative good agreement with results from inelastic helium scattering[19,20]), our value for β_4 appears to be a factor of 2 larger, well outside quoted errors, even when the deformation values are linearly scaled to account for the different radii[45]). Our results are in better agreement with electron scattering results[41]).

Recently J. Raynal has performed a coupled-channels calculation (using a new program which includes a search routine) on the ^{20}Ne data[46]). By letting all parameters vary including the β_2 and β_4 deformations, and doing a search on all cross sections and analyzing powers for the 0^+, 2^+ and 4^+ in ^{20}Ne, the calculations yield final β_2 and β_4 deformations equal to 0.42 and 0.27 respectively.

The optical model parameters were almost unchanged with the exception of the spin-orbit diffuseness, which reduced to ~ 0.10 fm.

The CC results for the lowest 0^+, 2^+ and 4^+ states in ^{22}Ne are given in figs. 10 and 11. As can be seen from these figures, the cross sections as well as the analyzing powers favor a rather small value for the Y_4 deformation ($\beta_4 = 0.05$) of ^{22}Ne, while the value found for β_2 is similar to that for ^{20}Ne. Similar conclusions have also been obtained from 40 MeV proton scattering work on ^{20}Ne and ^{22}Ne[28]), as well as from alpha scattering experiments[19]).

Figure 10 shows again that the calculations strongly support the full Thomas form and the analyzing powers for the 0^+, 2^+ and 4^+ states are very well reproduced using this type of deformed spin-orbit term together with the optical model parameters of Table 2. It has been suggested on a theoretical basis[14]) that the best agreement with the data is reached when the spin-orbit deformation is taken to be greater then that of the central potential. We have found this to be a necessity in the case of ^{20}Ne and ^{22}Ne, where the best fits for the analyzing power were obtained when the ratio of the two deformations was taken to be 2. Comparison between microscopic and macroscopic treatments by Raynal[16]) indicates that this ratio is directly related to the nuclear structure of the excited states and hence some variations may be expected throughout the s-d shell. However, no calculations have yet been performed to predict the size of the effect expected for ^{20}Ne and ^{22}Ne. As will be seen later, good fits for ^{32}S and ^{28}Si can be obtained without having to increase the deformation of the spin-orbit potential with respect to the central potential.

5.2. COUPLED-CHANNELS CALCULATIONS: ^{16}O, ^{28}Si AND ^{32}S

Previous CC calculations done on the 17.5 MeV proton inelastic scattering data of Crawley[47]) have used oblate shapes for ^{28}Si and ^{32}S and large hexadecapole moments ($\beta_4 = 0.25$)[18]). Even if the rotational character of the ^{28}Si lowest 0^+, 2^+, 4^+ states is well established[48,49]) and the oblate shape confirmed[19,41]), the situation for ^{32}S is much more complicated[49]). Recent measurements of the quadrupole moments of the first excited states of even-even nuclei in the 2s-1d shell[35]) brought additional evidence for the oblate shape for ^{28}Si ($Q_0 < 0$). The surprising change in sign of Q_0 between ^{28}Si and ^{32}S appears to indicate a serious difficulty in predicting deformations of nuclei in this mass region. Several recent experiments have suggested that the levels of ^{32}S up to an excitation of 5 MeV are well explained on the assumption that ^{32}S is an almost spherical vibrational nucleus[49-51]). Since a recent α-γ angular correlation experiment[52]) on ^{28}Si and a (α,α') experiment[53]) on ^{32}S yields very surprising prolate ($\beta_2 > 0$) quadrupole deformation for these nuclei, it appears necessary to analyse these data both with the vibrational (collective model) and the rotational model with oblate and prolate deformations.

The CC calculations for the $K = 0^+$ ground state band (2^+ and 4^+ states) of ^{28}Si using both the vibrational model and the rotational model (prolate shape) are presented in fig. 12. Although the full Thomas term was used, the agreement to the data is poor. The CC calculations results using the full Thomas term and rotational (oblate deformation) are presented in figs. 13 and 14. Very good fits to cross sections and polarizations are obtained with a negative quadrupole deformation $\beta_2 = -0.40$ and a positive hexadecapole β_4 deformation equal to +0.10. The values of these deformations are quite different from

those previously determined[18]) using only the Crawley cross sections, but are in very good agreement with the (α,α')[19]) and (e,e')[41]) results and with microscopic α-cluster model calculations[39]), as well as with some recent polarization data at 25.25 MeV[54]). The comparison of curves 1 and 3 of figs. 13 and 14 shows the sensitivity of the theory to the β_4 deformation parameter. If β_4 is increased, the fits deteriorates quite rapidly. Since no cross sections for the 4^+ state in ^{28}Si were available, the value determined for the β_4 deformation is less precise; and error of ± 0.04 is assigned to the β_4 determined in ^{28}Si. All calculations presented in the figures, if not otherwise specified, used the full Thomas term for the deformed spin-orbit term. Coulomb excitation was also generally included although it has a small effect. Curve 2 shows the results when $\beta_{so}/\beta_{central}$ were equal to unity; curve 1 shows the results when the deformation lengths ($\beta_{LS}\ r_{LS}/\beta_{central}\ r_o$) were equal to unity. In the latter case, $\beta_{LS}/\beta_{central}$ is equal to 1.29. Even better fits could be obtained by increasing the ratio up to 1.5[54]), or to 2.0 as for ^{20}Ne, but the optimum value of β_4 did not change significantly.

Coupled-channels calculations for ^{32}S are presented in figs. 15, 16 and 17 using either the rotational model (fig. 15) or the vibrational model (figs. 16 and 17). As seen in fig. 15, it is quite difficult to distinguish between oblate and prolate deformation. The overall χ^2 slightly favors a prolate shape for ^{32}S ($\beta_2 > 0$), but when only polarization data are taken into account, the oblate solution is the best ($\beta_2 = -0.30$). Since the overall χ^2 is 1946 in the case of $\beta_2 = +0.30$ and only 2126 when $\beta_2 = -0.30$, a definite assignment of the signs of the deformation for ^{32}S is not possible on the basis of our data. Addition of a hexadecapole deformation β_4 to the quadrupole

deformation β_2 has little effect if β_4 is small (up to around 0.1), but it quickly destroys the fits to the data when it is increased above this value. Therefore we conclude that the hexadecapole deformation is absent or very small in the ground state band of ^{32}S.

Figures 16 and 17 present CC results using a vibrational model with either 0^+, 2^+ coupling and a deformation parameter of +0.3 for the 2^+, or a 0^+, 2^+ and 3^- coupling with a deformation for the 3^- equal to +0.41. The fits to the data are quite good, especially in the case of the $(0^+,2^+)$ coupling. They are essentially equivalent to those of the rotational model since the overall χ^2 is 2155. It has been suggested from recent experiments such as $(p,p')^{51}$), $(d,d')^{49}$) or by lifetime measurements[55]) that the upper half of the s-d shell nuclei may have a spherical structure, although this behavior is not reproduced by Hartree-Fock calculations[38]). The energy level spacings of ^{32}S indeed show considerable deviation from the rotational model pattern and more resemble a vibrational spectrum. From our data and analysis, it is impossible to choose between rotational or vibrational structure. More precise data, especially for the 4^+ state at 4.47 MeV or for the next 0^+, 2^+, 4^+ states which may be the two phonon states in the vibrational model, are needed.

Finally, the results of CC calculations for the 2^+ states at 6.92 MeV and the 3^- state at 6.13 MeV for ^{16}O are presented in fig. 17. Very good fits for 3^- state and an acceptable fit for the2^+ state for this nucleus are obtained in the framework of the collective model (vibrational) with the full Thomas term and a deformation parameter of +0.50 for the 3^- and 0.2 for the 2^+.

6. Conclusions

In summary, coupled-channels calculations using permanently deformed nuclear wave functions reproduce well our cross section and analyzing power data on the elastic and inelastic scattering of polarized protons exciting the ground state rotational bands of ^{20}Ne, ^{22}Ne and ^{28}Si. Table 3 summarizes the nuclear deformations determined from the CC calculations. Prolate shapes of ^{20}Ne and ^{22}Ne and an oblate shape of ^{28}Si are strongly preferred. The situation for ^{32}S is not so clear, since the calculations could not decide between oblate-prolate deformation or for a spherical vibrational structure, although the overall best χ^2 slightly favors a prolate deformation.

Hexadecapole deformations found for ^{22}Ne and ^{28}Si are in good agreement with recent (α,α')[19], (e,e')[41] experiments and with theoretical calculations[39]. Large differences for the Y_4 moment of ^{20}Ne appear in the literature, especially in scattering experiments using α or ^{3}He particles as probes[19,20].

Finally, we have shown over a wide range of nuclei that the use of the Blair-Sherif form for the deformed spin-orbit interaction, in conjunction with a coupled-channels reaction calculation, is necessary to explain our cross-section and asymmetry results. However, we are gratified that calculations of the deformation parameters using simple forms of the interaction do not greatly change the results.

References

1) C. Glashausser, R. de Swiniarski, J. Thirion and A. D. Hill, Phys. Rev. 164 (1967) 1437

2) C. Glashausser, R. de Swiniarski, J. Goudergues, R. M. Lombard, B. Mayer, and J. Thirion, Phys. Rev. 184 (1969) 1217

3) A. G. Blair, C. Glashausser, R. de Swiniarski, J. Goudergues, R. Lombard, B. Mayer, J. Thirion, and P. Vaganov, Phys. Rev. C1 (1970) 444

4) R. M. Craig, J. C. Dore, G. W. Greenlees, J. Lowe, and D. L. Watson, Nucl. Phys. 83 (1966) 493; D. J. Baugh, M. J. Kenny, J. Lowe, D. L. Watson, and H. Wojciechowski, Nucl. Phys. A99 (1967) 203

5) O. Karban, J. Lowe, P. D. Greaves, and V. Hnizdo, Nucl. Phys. A133 (1969) 255; A141 (1970) 675

6) O. Karban, P. D. Greaves, V. Hnizdo, J. Lowe and G. W. Greenless, Nucl. Phys. A147 (1970) 461

7) M. P. Fricke, E. E. Gross, and A. Zucker, Phys. Rev. 163 (1967) 1153; M. P. Fricke, Thesis O.R.N.L., unpublished

8) V. E. Lewis, E. J. Burge, A.A. Rush and D. A. Smith, Nucl. Phys. A101 (1967) 589

9) C. Glashausser and J. Thirion, Advances in Nuclear Physics, 2 (1969) 79

10) Polarization Phenomena in Nuclear Reactions, Proceedings of the Third International Symposium, Madison 1970, ed. by H. H. Barschall and W. Haeberli (additional references can be found here as well as in ref. 9)

11) J. Lowe, Nucl. Phys. A162 (1971) 438

12) J. L. Escudié, A. Tarrats, and J. Raynal, Proceedings of the Third International Symposium on Polarization Phenomena in Nuclear Reactions, Madison 1970, ed. by H. H. Barschall and W. Haeberli, p. 705

13) P. D. Greaves, V. Hnizdo, J. Lowe, and O. Karban, Proceedings of the Third International Symposium on Polarization Phenomena in Nuclear Reactions, Madison 1970, ed. by H. H. Barschall, and W. Haeberli, p. 697; Nucl. Phys. A179 (1972) 1

14) H. Sherif and J. S. Blair, Phys. Letters 26B (1968) 489

15) H. Sherif, Ph.D. Thesis, University of Washington (1968) unpublished; H. Sherif and R. de Swiniarski, Phys. Letters 28B (1968) 96; H. Sherif, Nucl. Phys. A131 (1969) 532; H. Sherif and J. S. Blair, Nucl. Phys. A140 (1970) 33

16) J. Raynal, Proceedings of the Symposium on Nuclear Reactions Mechanisms and Polarizations Phenomena, Laval University, Quebec 1969, p. 75; J. Raynal, Lectures presented at the Nuclear Theory Course, Trieste, January-March 1971; D.Ph/t n° 71/1, Saclay (unpublished)

17) R. de Swiniarski, A. D. Bacher, F. G. Resmini, G. R. Plattner, D. L. Hendrie, and J. Raynal, Phys. Rev. Letters 28 (1972) 1139; A. D. Bacher, R. de Swiniarski, D. L. Hendrie, A. Luccio, G. R. Plattner, F. G. Resmini, and J. Sherman in the Proceedings of the Third International Symposium on Polarization Phenomena in Nuclear Reactions, Madison 1970, ed. by H. H. Barschall and W. Haeberli (The University of Wisconsin Press, Madison 1971), p. 708

18) R. de Swiniarski, C. Glashausser, D. L. Hendrie, J. Sherman, A. D. Bacher, and E. A. McClatchie, Phys. Rev. Letters 23 (1969) 317

19) H. Rebel, G. W. Schweimer, J. Specht, G. Schatz, R. Löhken, D. Habs, G. Hauser, and H. Klewe-Nebenius, Phys. Rev. Letters 26 (1971) 1190 and Nucl. Phys. A182 (1972) 145; J. Specht, H. Rebel, G. Schatz, G. W. Schweimer, G. Hauser, and R. Löhken, Nucl. Phys. A143 (1970) 373; J. W. Frickey, K. A. Eberhard, and R. H. Davis, Phys. Rev. C4 (1971) 434

20) K. W. Kemper, D. S. Haynes, and N. R. Fletcher, Phys. Rev. C4 (1971) 408

21) R. de Swiniarski, J. Sherman, A. D. Bacher, C. Glashausser, D. L. Hendrie, and E. A. McClatchie, Bull. Am. Phys. Soc. 14 (1969) 531

22) H. S. Sandhu, J. M. Cameron, and W. F. McGill, Nucl. Phys. A169 (1971) 600; H. S. Sandhu, private communication; R. K. Cole, C. N. Waddell, R. R. Ditman, and H. S. Sandhu, Nucl. Phys. 75 (1969) 241

23) J. K. Dickens, D. A. Haner, and C. N. Waddell, Phys. Rev. 129 (1963) 743; Phys. Rev. 132 (1963) 2159

24) A. U. Luccio, D. J. Clark, D. Elo, P. Frazier, D. Morris, and M. Renkas, IEEE Trans. Nucl. Sci., NS-16 (1969) 110

25) D. J. Clark, A. U. Luccio, F. G. Resmini, and H. Meiner in Proceedings of the Fifth International Cyclotron Conference, Oxford (England), (Butterworth, London 1971) p. 610

26) R. M. Craig, J. C. Dore, G. W. Greenless, J. S. Lilley, J. Lowe, and P. C. Rowe, Nucl. Instr. Methods 30 (1964) 269

27) A. D. Bacher, G. R. Plattner, H. E. Conzett, D. J. Clark, H. Grunder, and W. F. Tivol in Proceedings of the Third International Symposium on Polarization Phenomena in Nuclear Reactions, Madison (1970), ed by H. H. Barschall and W. Haeberli, p. 569

28) D. Madland and N. M. Hintz, J. H. Williams Laboratory, Annual Report 1970, University of Minnesota, p. 23

29) We would like to thank Dr. C. Maples for using his fitting program "DER TAG"

30) D. L. Hendrie, N. K. Glendenning, B. G. Harvey, O. N. Jarvis, H. H. Duhm, J. Saudinos, and J. Mahoney, Phys. Letters 26B (1968) 127; N. K. Glendenning, D. L. Hendrie, and O. N. Jarvis, Phys. Letters 26B (1968) 131

31) J. M. Cameron, Ph.D. Thesis, University of California at Los Angeles, unpublished

32) "MAGALI" - A Fortran IV Program for automatic search in elastic scattering analysis with the nuclear optical model for spin 0, 1/2 and 1 particles by J. Raynal, DPh.T/69-42, Saclay

33) G. R. Satchler, Nucl. Phys. A92 (1967) 273

34) H. E. Gove in Proceedings of the International Conference on Nuclear Structure, Kingston (1960) (University Toronto Press, 1960) p. 436 and University of Rochester Report UR.NSRL-7 (1968)

35) A Bamberger, P. G. Bizzeti, and B. Povh, Phys. Rev. Letters 21 (1968) 1599; O. Häusser, B. W. Hooten, D. Pelte, T. K. Alexander, and H. C. Evans, Phys. Rev. Letters 22 (1969) 359; D. Schwalm and B. Povh, Phys. Letters 29B (1969) 103; D. Pelte, O. Häusser, T. K. Alexander, and H. C. Evans, Can. J. Phys. 47 (1969) 1929; K. Nakai, J. L. Quebert, F. S. Stephens, and R. Diamond, Phys. Rev. Letters 24 (1970) 903

36) S. Das Gupta and M. Harvey, Nucl. Phys. A94 (1967) 602; B. Castel and J. P. Sennen, Nucl. Phys. A127 (1969) 141; G. Ripka in Advances in Nuclear Physics, Vol. 1, ed. by M. Baranger and E. Vogt, Plenum Press, New York (1968)

37) C. Brihaye and G. Reidemeister, Nucl. Phys. A100 (1967) 65; H. G. Benson and B. H. Flowers, Nucl. Phys. A126 (1969) 305; B. Castel and J. C. Parikh, Phys. Rev. C1 (1970) 990; M. K. Pal and A. P. Stamp, Phys. Rev. 158 (1967) 924

38) A. L. Goodman, G. L. Struble, J. Bar-Touv, and A. Goswami, Phys. Rev. C2 (1970) 380; D. Gozz, Phys. Rev. C2 (1970) 1168

39) Y. Abgrall and E. Caurier in Symposium on Heavy Ion Reactions and Many Particle Excitations, Saclay, Septetember 1971, Journal de Physique, Colloque C-6, suppl. au n° 11-12, Nov.-Dec. 1971, p. 63; Y. Abgrall, B. Morand and E. Caurier, Nucl. Phys. A192 (1972) 372; Y. Abgrall, private communication

40) D. K. Olsen, T. Udagawa, T. Tamura, and R. E. Brown, Phys. Rev. C8 (1973) 608

41) Y. Horikawa, Y. Torizuka, A. Nakada, S. Mitsunobu, Y. Kojima, and M. Kimura, Phys. Letters 36B (1971) 9

42) M. P. Barbier, R. Lombard, J. M. Moss, and Y. Terrien, Phys. Letters 34B (1971) 386

43) N. K. Glendenning in International School of Physics Enrico Fermi, Course XL, Academic Press, New York (1967)

44) A. D. Hill, unpublished

45) D. L. Hendrie, Phys. Rev. Letters 31 (1973) 478

46) J. Raynal, private communication

47) G. M. Crawley, Ph.D. thesis, Princeton University, 1965, unpublished

48) M. M. Aleonard, D. Castera, P. Hubert, F. Leccia, P. Mennrath, and J. P. Thibaud, Nucl. Phys. A146 (1970) 90

49) M. C. Mermaz, C. A. Whitten, Jr., and D. A. Bromley, Phys. Rev. 187 (1969) 1466

50) J. P. Thibaud, M. M. Aleonard, D. Castera, P. Hubert, F. Leccia, and P. Mennrath, Nucl. Phys. A135 (1969) 281

51) R. Lombard, H. Kamitsubo, J. Raynal, and J. Gosset, Compt. Rend. Ac. Sc., Paris, 274 (1972) Serie B, 761

52) C. E. Ahlfeld, G. E. Assousa, R. A. Lasalle, W. J. Thomson, H.A. Van Ruisvelt, and N. P. Heydenburg, Nucl. Phys A191 (1972) 137

53) G. W. Schweimer, H. Rebel, G. Nowicki, G. Hauser, and R. Löhken, Phys. Letters 39B (1972) 627

54) R. de Swiniarski, H. E. Conzett, C. R. Lamontagne, B. Frois, and R. J. Slobodrian, Can. J. Phys. 51 (1973) 1293

55) G. T. Garvey, K. W. Jones, L. E. Carlson, D. A Hutcheon, A. G. Robertson, and D. F. H. Start, Nucl. Phys. A160 (1971) 25

Table 1

Nucleus	Search	V_o (MeV)	r_o (F)	a_o (F)	W_V (MeV)	W_D (MeV)	r_I (F)	a_I (F)	V_{LS} (MeV)	r_{LS} (F)	a_{LS} (F)	χ^2_σ	χ^2_p
^{20}Ne	σ + p	59.10	1.01	0.77	0.0	7.54	1.26	0.62	3.57	0.86	0.33	217	1290
^{22}Ne	σ + p	58.0	1.05	0.78	0.0	7.73	1.33	0.57	3.95	0.88	0.31	31	562
^{28}Si	σ + p	50.72	1.11	0.68	0.0	6.10	1.34	0.54	6.43	0.86	0.55	261	150
^{32}S	σ + p	53.87	1.09	0.73	0.0	6.3	1.34	0.63	7.30	0.74	0.91	84	98
^{16}O	σ + p	43.25	1.14	0.69	0.0	2.78	1.36	0.84	4.31	1.11	0.45	855	135

Table 2

Nucleus	V_o (MeV)	r_o (F)	a_o (F)	W_V (MeV)	W_D (MeV)	r_I (F)	a_I (F)	V_{LS} (MeV)	r_{LS} (F)	a_{LS} (F)
^{20}Ne	59.0	1.01	0.75	0.0	6.5	1.26	0.55	3.57	0.90	0.33
^{22}Ne	57.0	1.05	0.75	0.0	6.3	1.33	0.55	3.95	0.88	0.31
^{28}Si	50.72	1.11	0.68	0.0	6.10	1.34	0.54	6.43	0.86	0.55
^{32}S	53.87	1.09	0.73	0.0	6.3	1.34	0.63	7.30	0.74	0.91
^{16}O	43.25	1.14	0.69	0.0	2.78	1.36	0.84	4.31	1.11	0.45

Table 3

Values of deformation parameters and multipole moment from scattering of polarized protons

	^{20}Ne	^{22}Ne	^{28}Si	^{32}S
β_2	+0.47	+0.47	-0.40	(+)0.30
β_4	+0.28	+0.05	+0.10	-

Figure Captions

Figure 1 Measured analyzing power for the low-lying excited states in ^{20}Ne obtained by scattering of 24.5 MeV protons.

Figure 2 Measured analyzing power for the strongly excited states in ^{22}Ne obtained by scattering of 24.5 MeV protons.

Figure 3 Measured analyzing for the low-lying collective states in ^{28}Si and ^{32}S obtained by scattering of 30.3 MeV protons.

Figure 4 Measured analyzing power for several states in ^{16}O by scattering of 30.3 MeV protons.

Figure 5 Optical model predictions for the elastic cross sections and polarization for ^{20}Ne and ^{22}Ne. The parameters are those of Table I.

Figure 6 Optical model predictions for the elastic cross sections and polarization for ^{28}Si and ^{32}S. Parameters of Table I were used.

Figure 7 Optical model prediction for the elastic cross section and polarization for ^{16}O. The parameters of Table I were used.

Figure 8 Coupled-channels calculations (rotational model) for the measured analyzing power for the first 0^+, 2^+ and 4^+ states in ^{20}Ne with and without the full Thomas term. Optical model parameters of Table II were used.

Figure 9 Experimental cross sections for the 0^+, 2^+ and 4^+ states in ^{20}Ne with coupled-channels calculations (rotational model) and the full Thomas term. Optical model parameters of Table II were used.

Figure 10 Measured analyzing power for the first 0^+, 2^+ and 4^+ states in ^{22}Ne with some coupled-channels calculations (rotational model) with and without the full Thomas term. Optical model parameters of Table II were used.

Figure 11 Experimental cross sections for the 0^+, 2^+ and 4^+ states in ^{22}Ne with coupled-channels calculations (rotational model) and the full Thomas term. Optical model parameters of Table II were used.

Figure 12 Coupled-channels calculations for the cross sections and analyzing power for the 2^+ and 4^+ states in ^{28}Si (rotational and vibrational model) with the full Thomas term. Optical model parameters of Table II were used.

Figure 13 Coupled-channels calculations for the experimental cross sections (rotational model) for the ground states $K = 0^+$ band in ^{28}Si with the full Thomas term. Optical model parameters of Table II were used.

Figure 14 Coupled-channels calculations with the full Thomas term and the rotational model for the measured analyzing power for the $K = 0^+$ band in ^{28}Si. Optical model parameters of Table II were used

Figure 15 Coupled-channels calculations for the first 0^+, 2^+ states in ^{32}S using the full Thomas with $\beta_{LS} = \beta_{central}$ and a rotational model with $\beta_2 = \pm$ 0.30 and optical model parameters of Table II.

Figure 16 Coupled-channels calculations for the cross sections for the strongly low-lying excited states in ^{32}S using a vibrational model, the full Thomas term with $\beta_{LS} = \beta_{central}$ and optical model parameters of Table II. Calculations were done by coupling either the 0^+, 2^+ or the 0^+, 2^+, 3^- states. Deformations parameters of 0.30 for the 2^+ and 0.41 for the 3^- were used.

Figure 17 Coupled-channels calculations for the measured analyzing power for the low-lying excited states in ^{32}S using a vibrational model, the full Thomas term with $\beta_{LS} = \beta_{central}$, and optical model parameters of Table II. Calculations were done by coupling either the 0^+, 2^+ or the 0^+, 2^+ and 3^- states. Deformations parameters of 0.30 for the 2^+ and 0.41 for the 3^- were used.

Figure 18 Coupled-channels calculations for the cross sections and analyzing power for the 2^+ state at 6.92 MeV and the 3^- state at 6.13 MeV in O^{16}. Full Thomas term, optical model parameters vibrational model and deformation parameters of + 0.50 for the 3^- and 0.2 for the 2^+ were used.

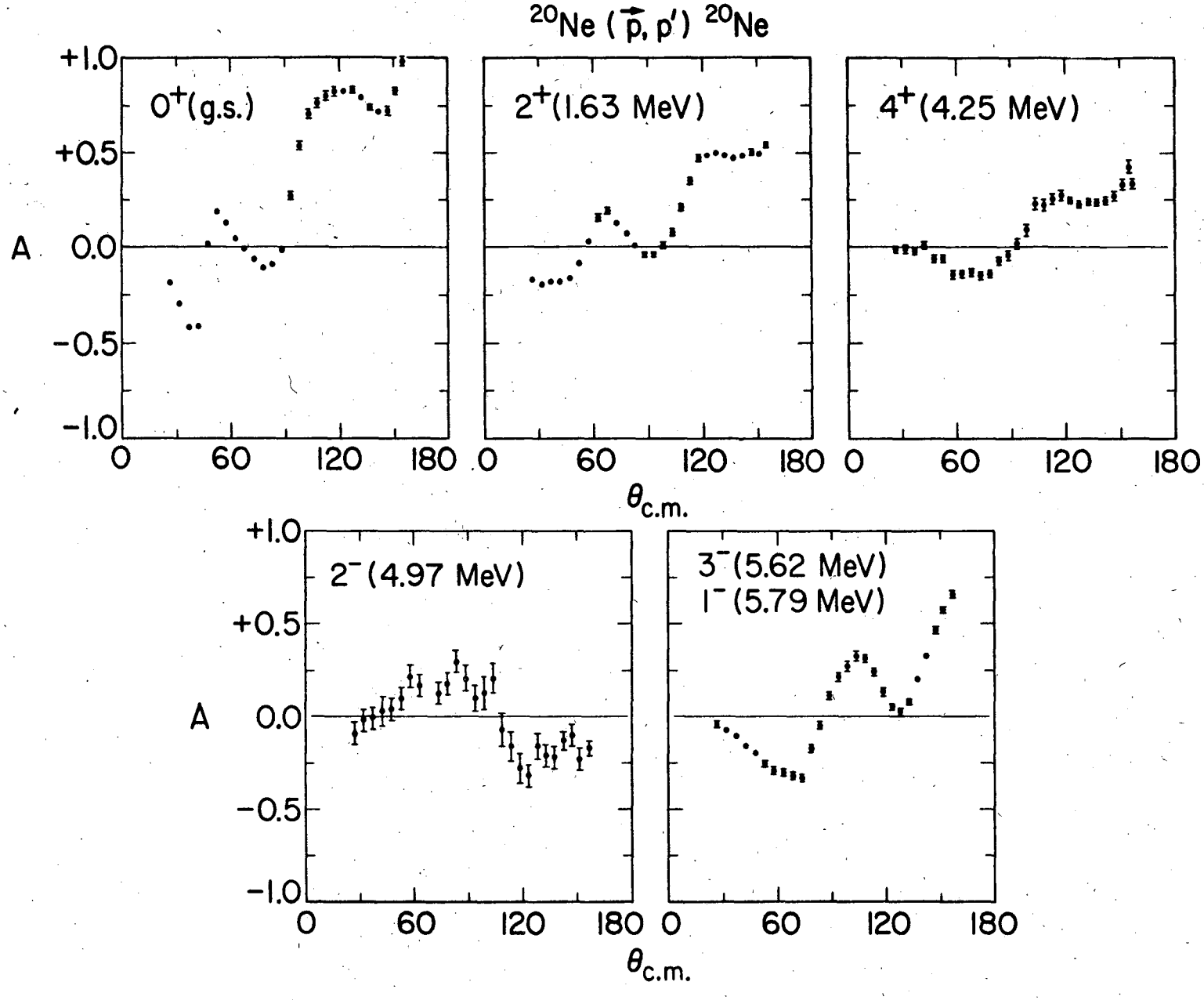

XBL704-2679

Fig. 1.

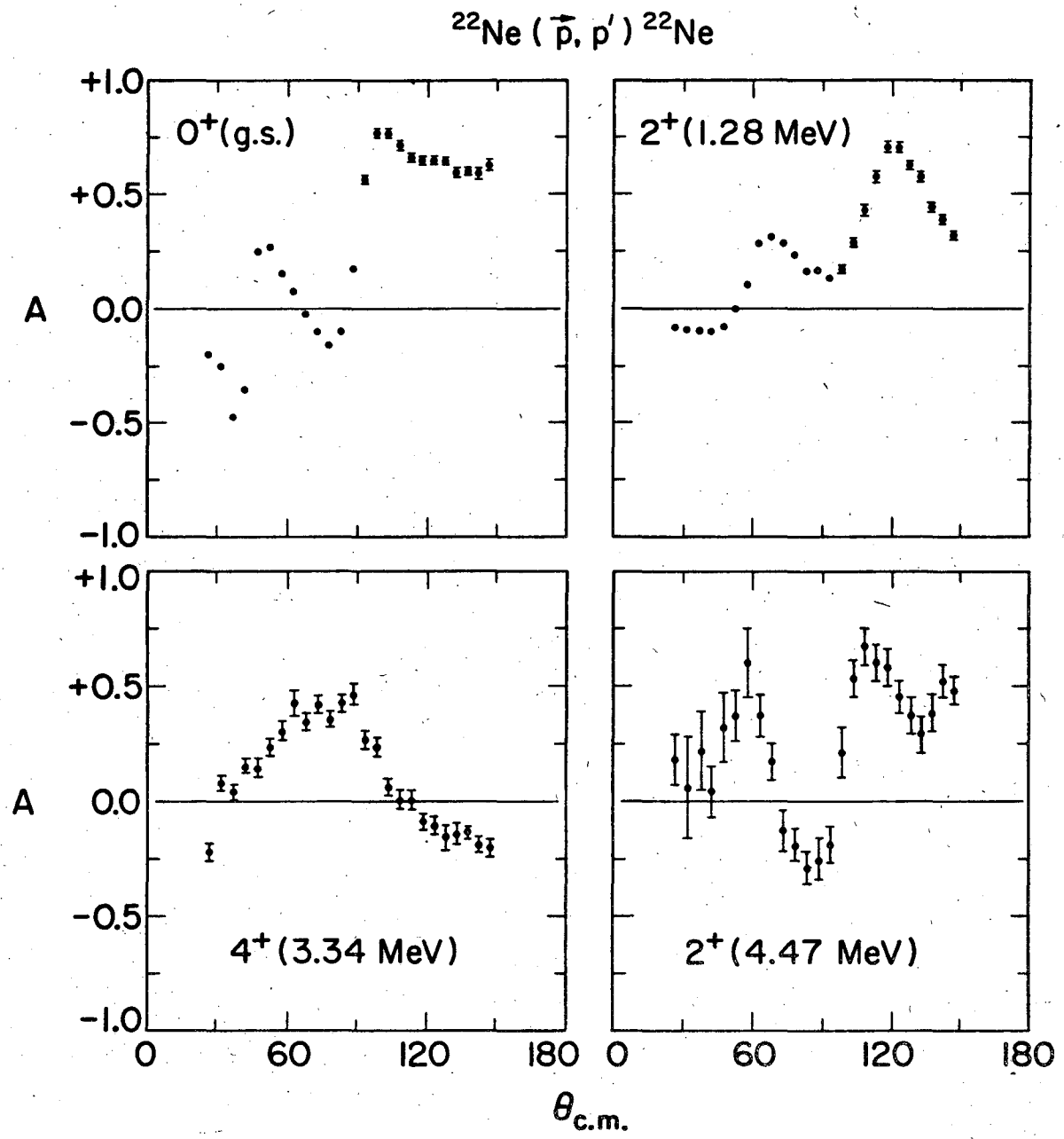

XBL704-2677

Fig. 2.

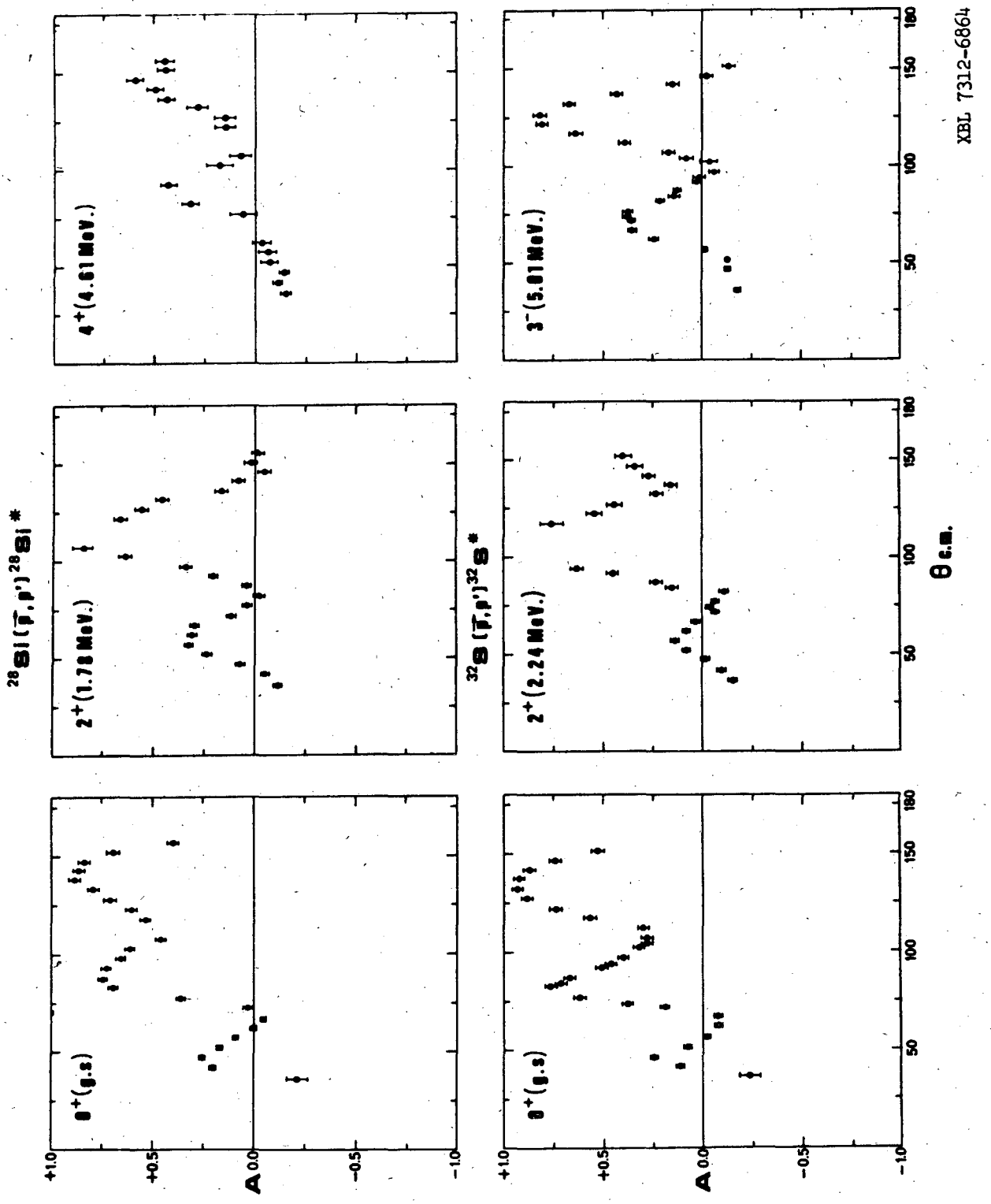
$^{28}Si(\vec{p},p')^{28}Si^*$
$^{32}S(\vec{p},p')^{32}S^*$
0^+(g.s)
2^+(1.78 MeV.)
4^+(4.61 MeV.)
2^+(2.24 MeV.)
3^-(5.01 MeV.)
A
$\theta_{c.m.}$
+1.0
+0.5
0.0
-0.5
-1.0
50
100
150
180
XBL 7312-6864

Fig. 3.

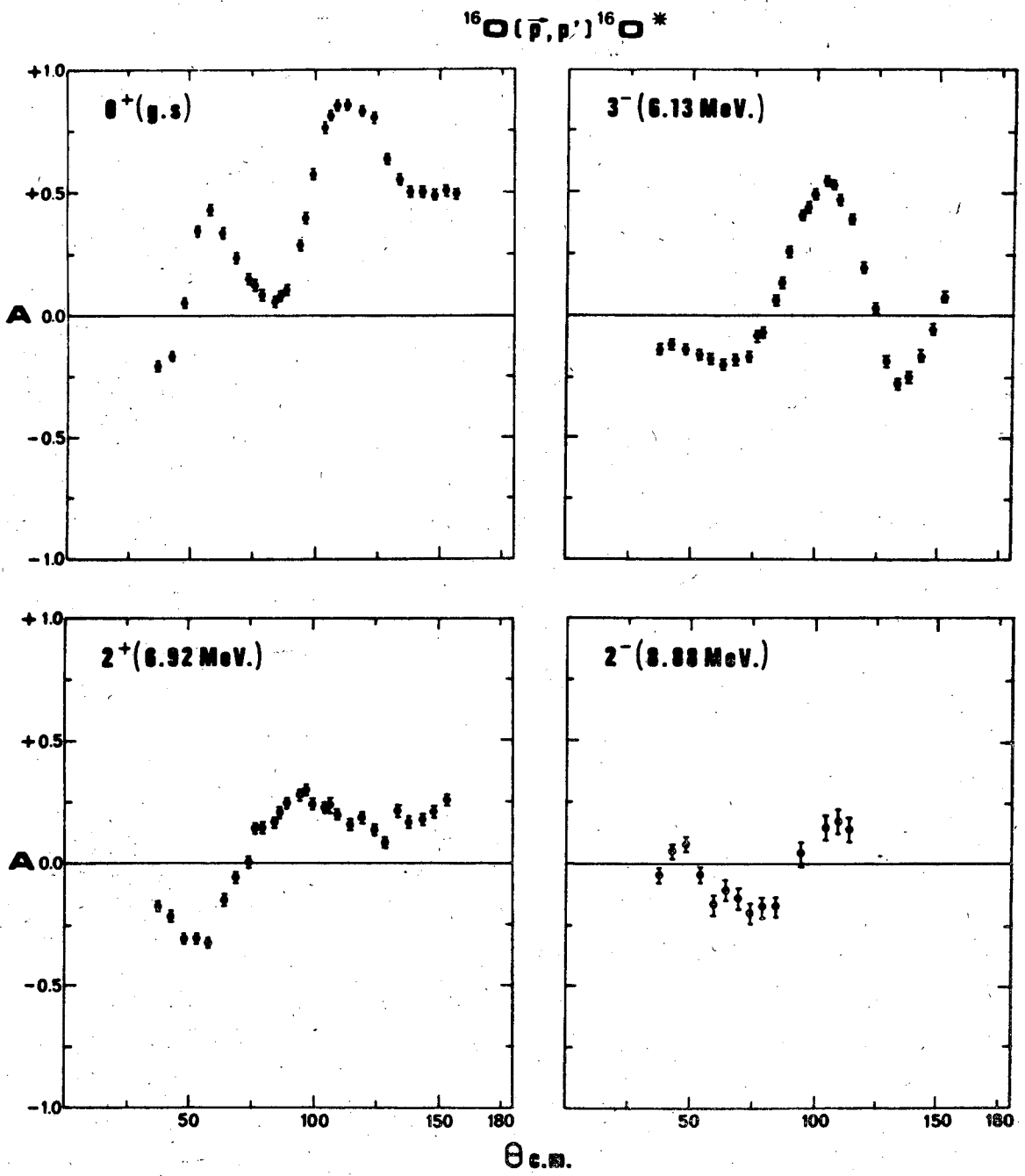

XBL 7312-6865

Fig. 4.

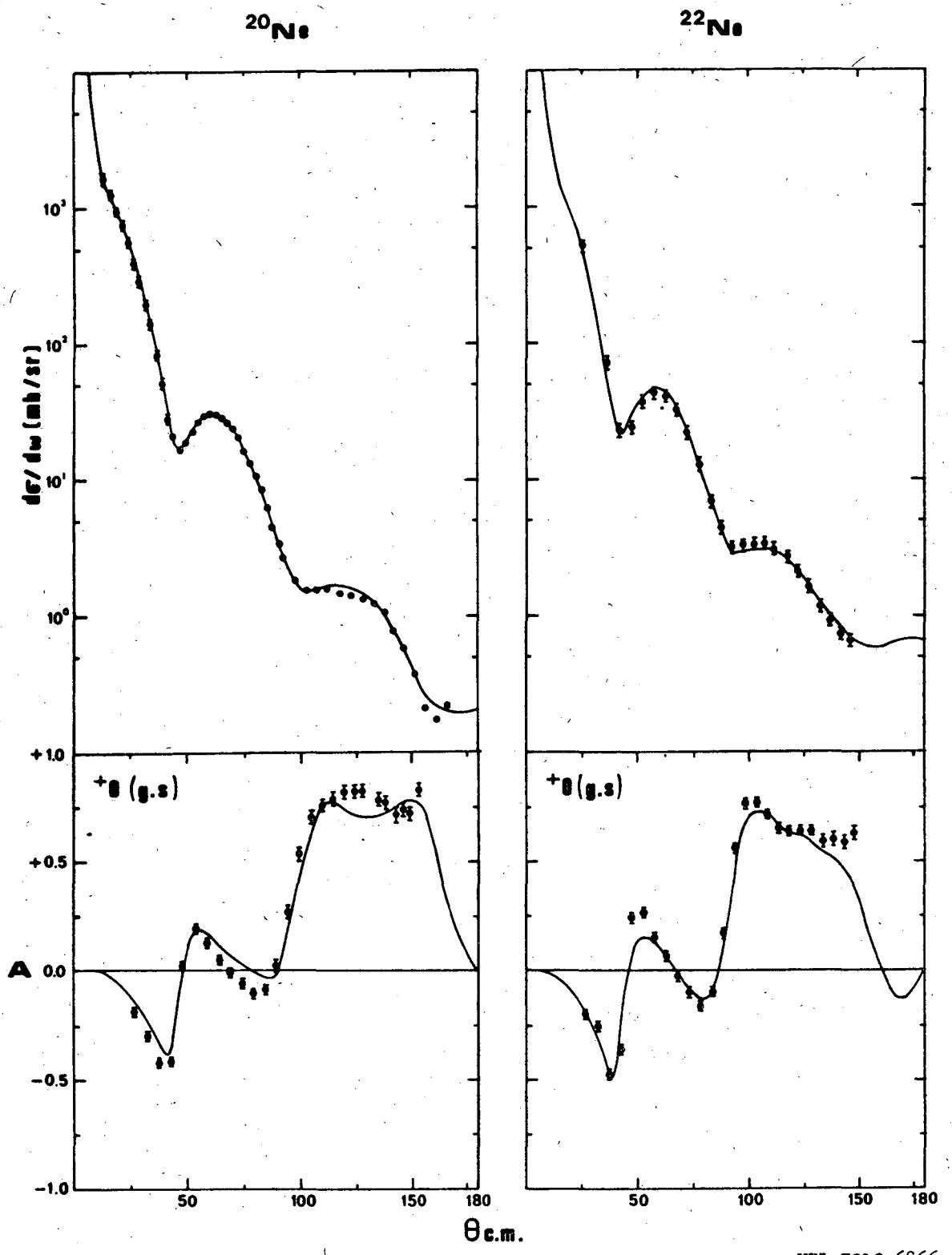
^{20}Ne
^{22}Ne
dσ/dω (mb/sr)
10^3
10^2
10^1
10^0
+1.0
+0.5
0.0
-0.5
-1.0
A
+θ (g.s)
+θ (g.s)
50
100
150
180
θc.m.
XBL 7312-6866

Fig. 5.

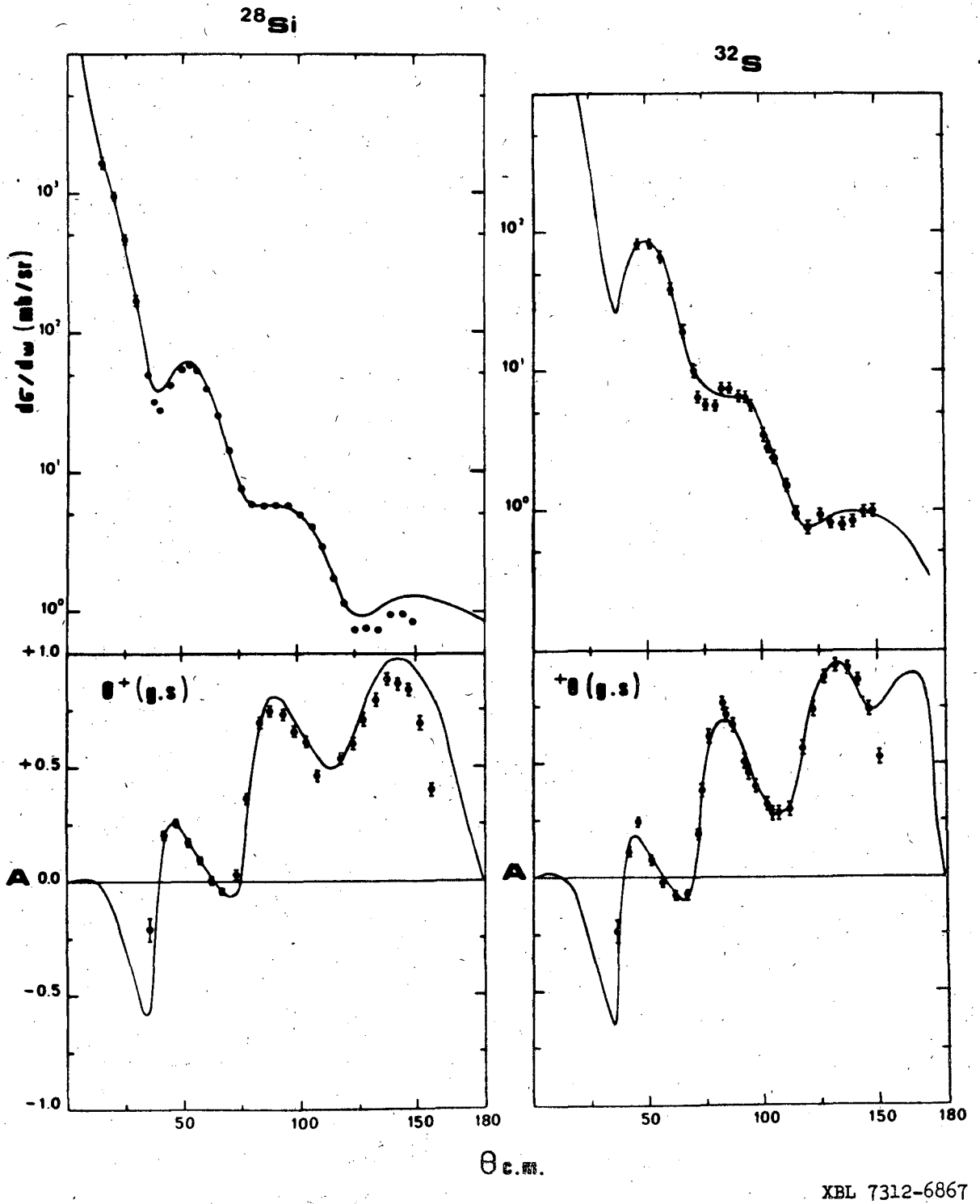

XBL 7312-6867

Fig. 6.

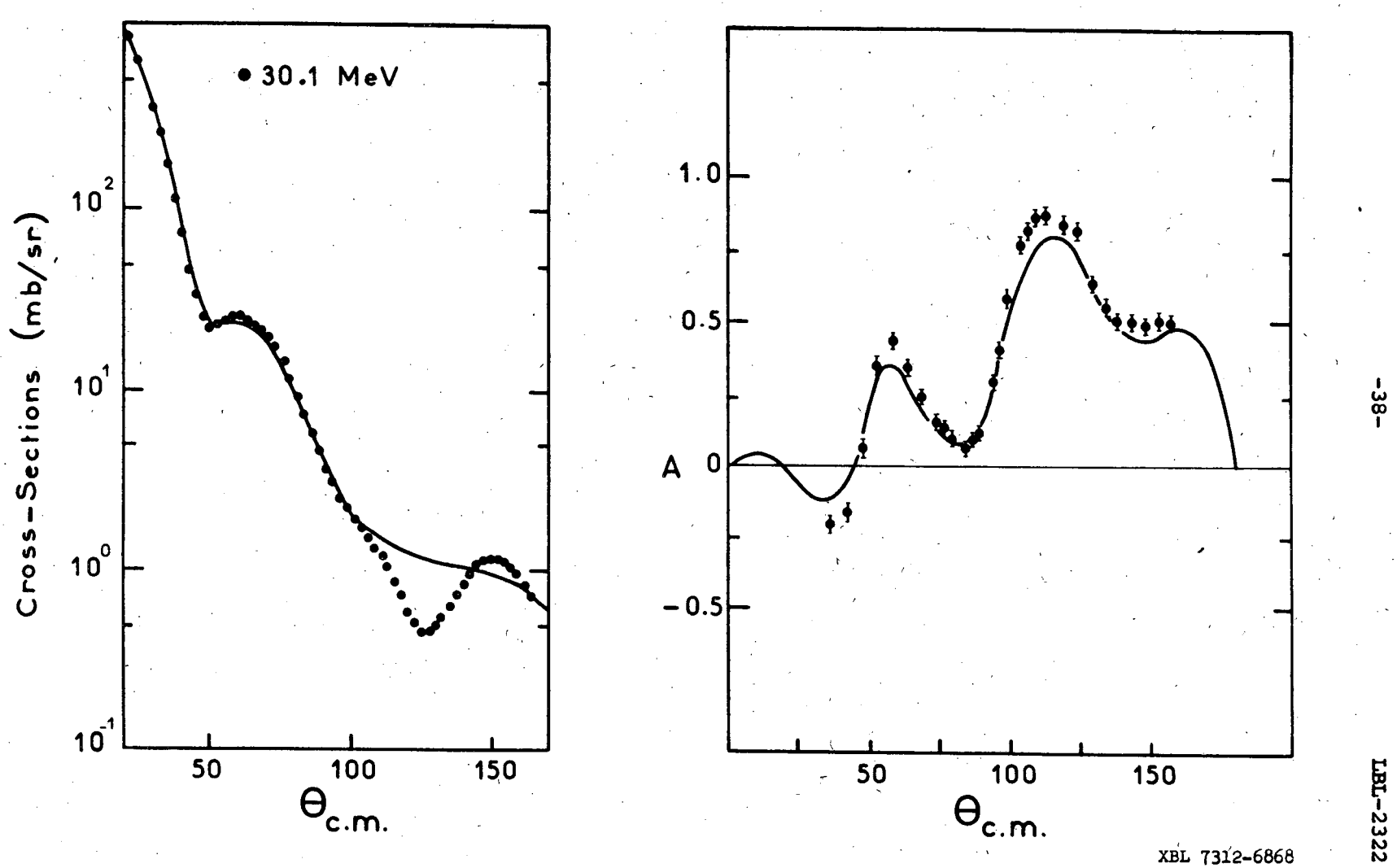
$^{16}O(p,p)^{16}O$
• 30.1 MeV
Cross-Sections (mb/sr)
10^2
10^1
10^0
10^{-1}
50
100
150
$\Theta_{c.m.}$
1.0
0.5
A 0
-0.5
50
100
150
$\Theta_{c.m.}$
XBL 7312-6868

Fig. 7.

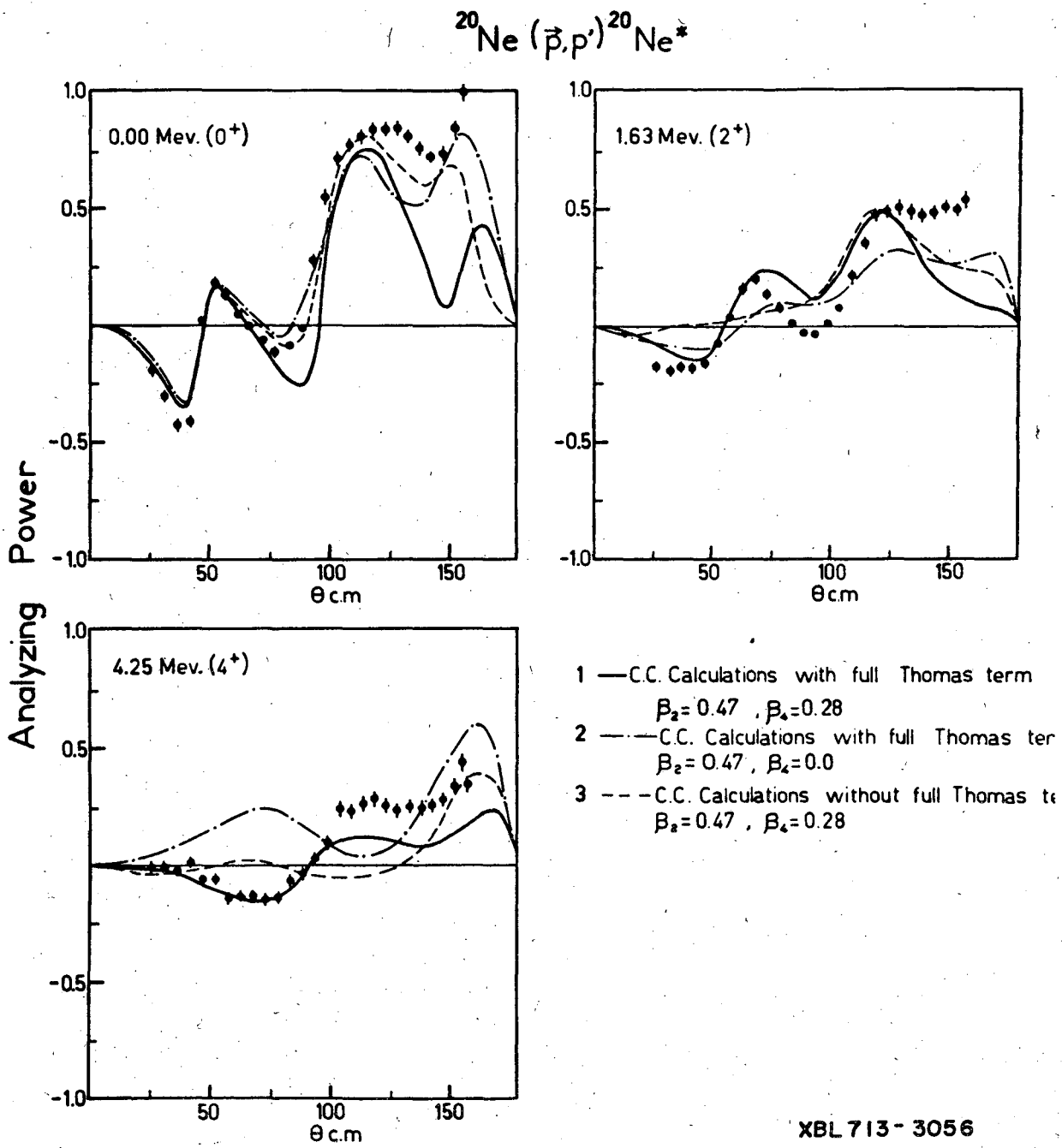
$^{20}Ne(\vec{p},p')^{20}Ne^*$
0.00 Mev. (0^+)
1.63 Mev. (2^+)
4.25 Mev. (4^+)
Analyzing Power
θ c.m
1 —C.C. Calculations with full Thomas term
$\beta_2 = 0.47$, $\beta_4 = 0.28$
2 —·—C.C. Calculations with full Thomas ter
$\beta_2 = 0.47$, $\beta_4 = 0.0$
3 – – –C.C. Calculations without full Thomas te
$\beta_2 = 0.47$, $\beta_4 = 0.28$
XBL 713-3056

Fig. 8.

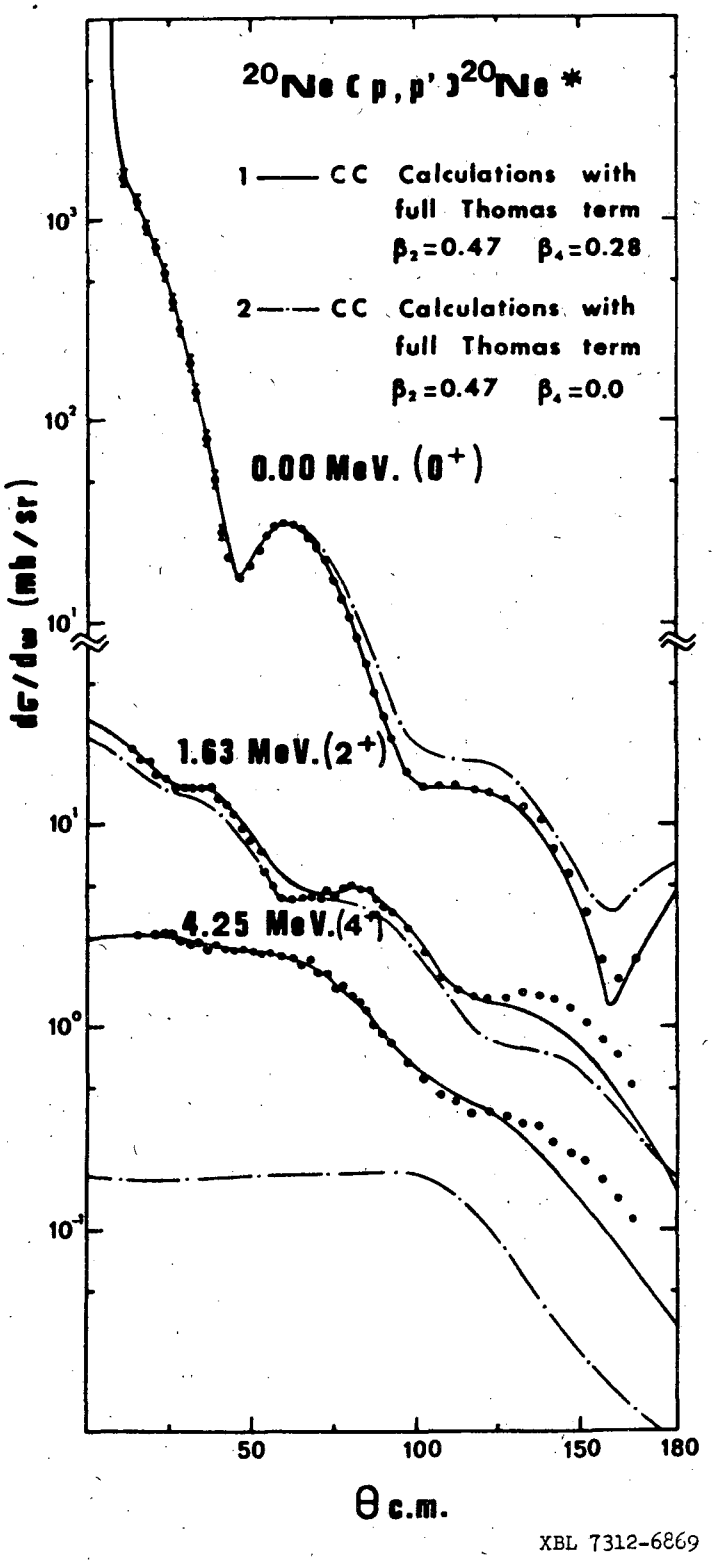
$^{20}Ne(p,p')^{20}Ne^*$
1 —— CC Calculations with full Thomas term $\beta_2=0.47$ $\beta_4=0.28$
2 —·— CC Calculations with full Thomas term $\beta_2=0.47$ $\beta_4=0.0$
0.00 MeV. (0^+)
1.63 MeV.(2^+)
4.25 MeV.(4^+)
$d\sigma/d\omega$ (mb/sr)
10^3
10^2
10^1
10^1
10^0
10^{-1}
50
100
150
180
θ c.m.
XBL 7312-6869

Fig. 9.

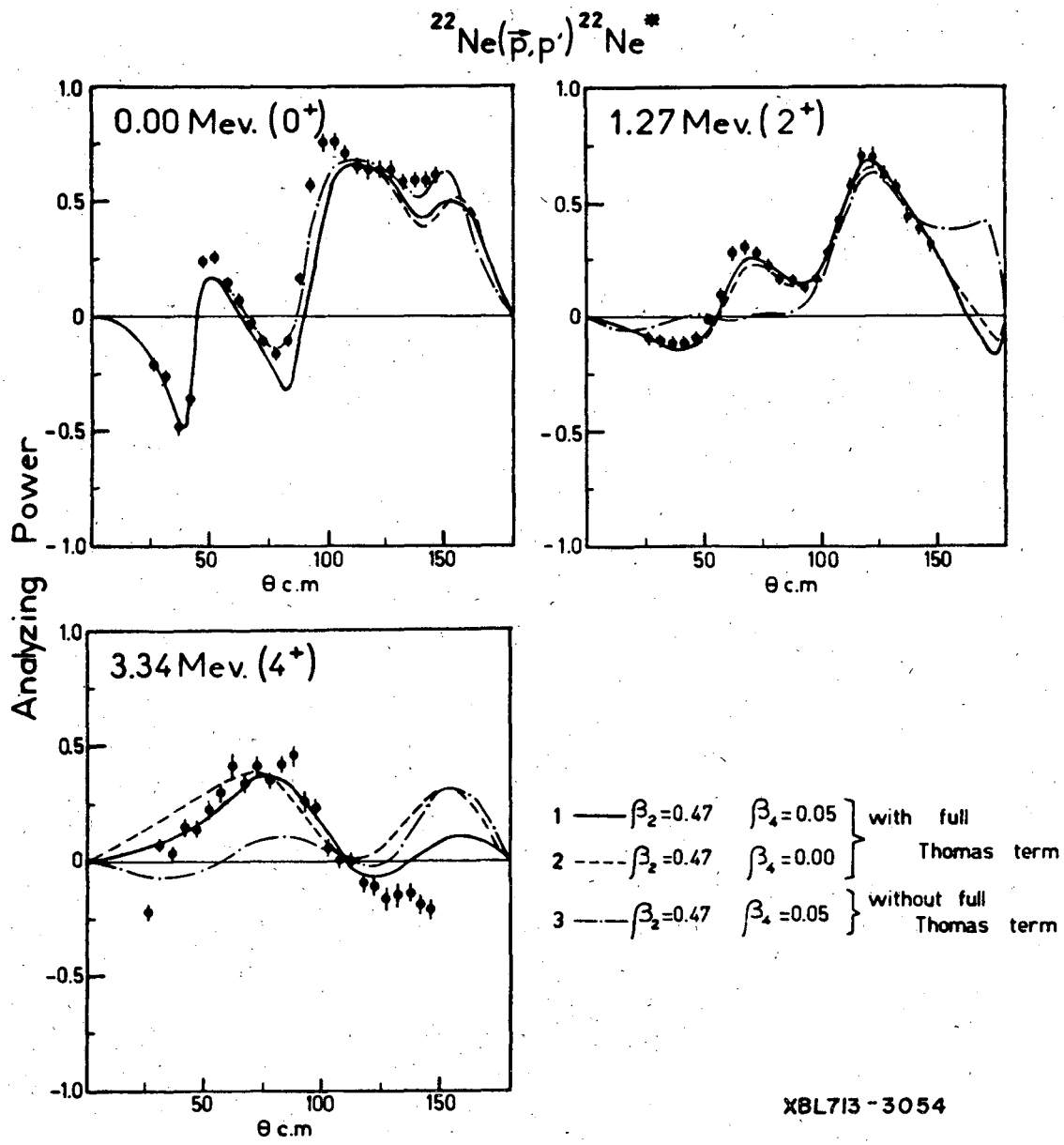
$^{22}Ne(\vec{p},p')^{22}Ne^{*}$
0.00 Mev. (0^+)
1.27 Mev. (2^+)
3.34 Mev. (4^+)
Analyzing Power
θ c.m
1 —— β_2=0.47 β_4=0.05 } with full Thomas term
2 ---- β_2=0.47 β_4=0.00 }
3 —·— β_2=0.47 β_4=0.05 } without full Thomas term
XBL713-3054

Fig. 10.

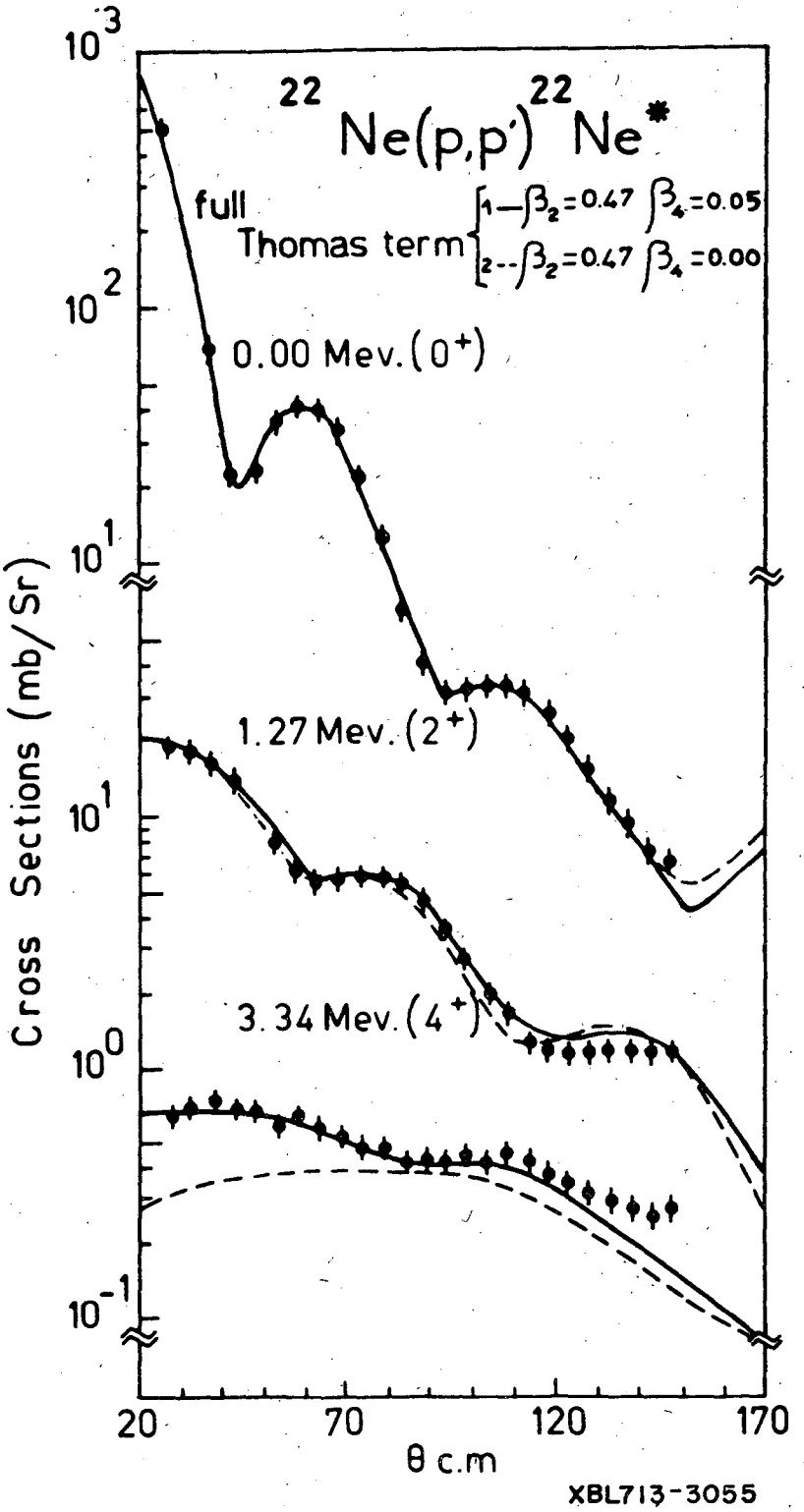
$^{22}Ne(p,p')^{22}Ne^*$
full
Thomas term
$\beta_2=0.47$ $\beta_4=0.05$
$\beta_2=0.47$ $\beta_4=0.00$
0.00 Mev. (0^+)
1.27 Mev. (2^+)
3.34 Mev. (4^+)
Cross Sections (mb/Sr)
10^3
10^2
10^1
10^1
10^0
10^{-1}
20
70
120
170
θ c.m
XBL713-3055

Fig. 11.

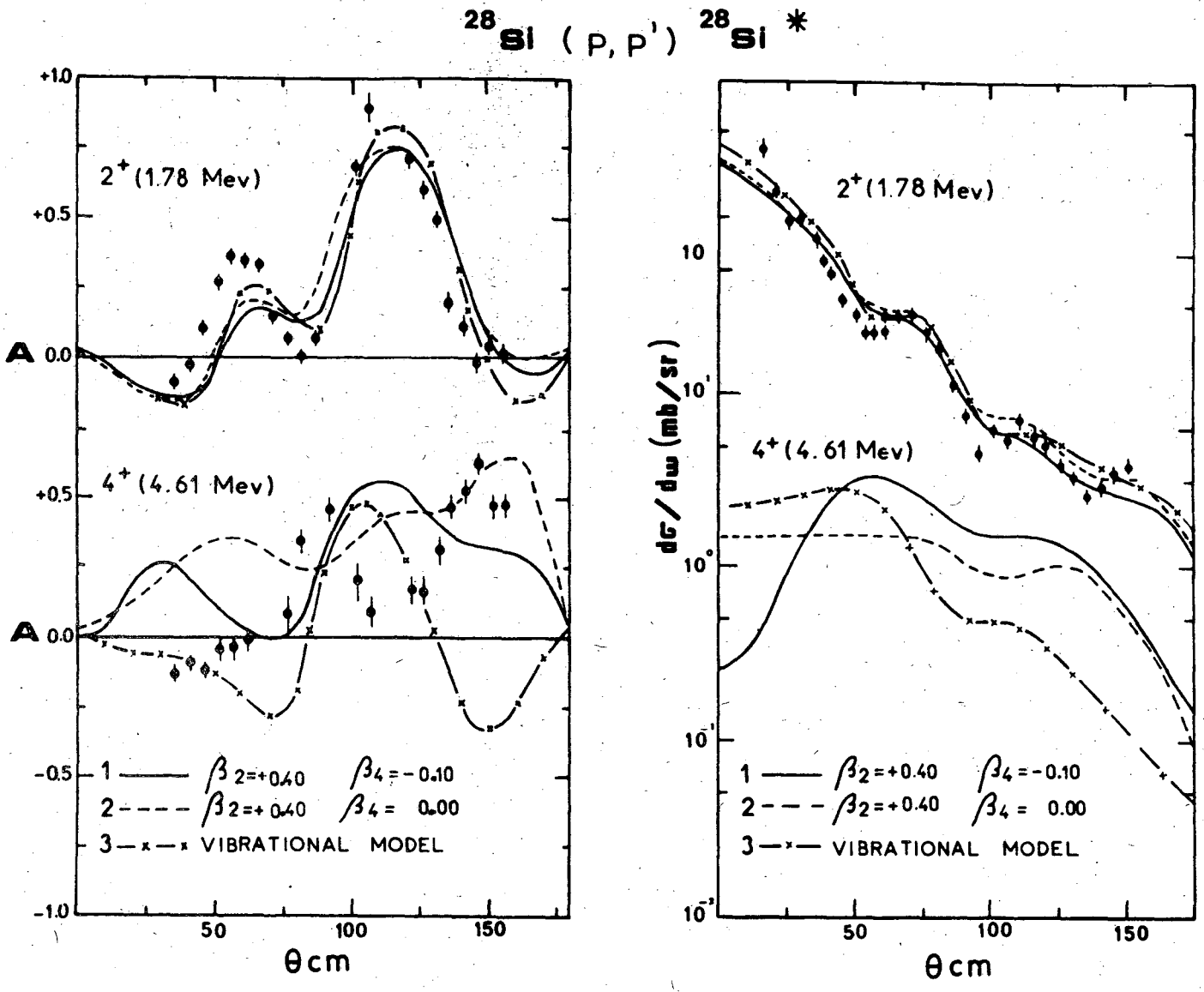
28Si (P, P') 28Si *
2+ (1.78 Mev)
4+ (4.61 Mev)
A
+1.0
+0.5
0.0
-0.5
-1.0
1 —— β2=+0.40 β4=-0.10
2 - - - - β2=+0.40 β4= 0.00
3 —x—x VIBRATIONAL MODEL
50
100
150
θcm
dσ/dω (mb/sr)
10
10'
10°
10⁻¹
10⁻²
XBL 7312-6870

Fig. 12.

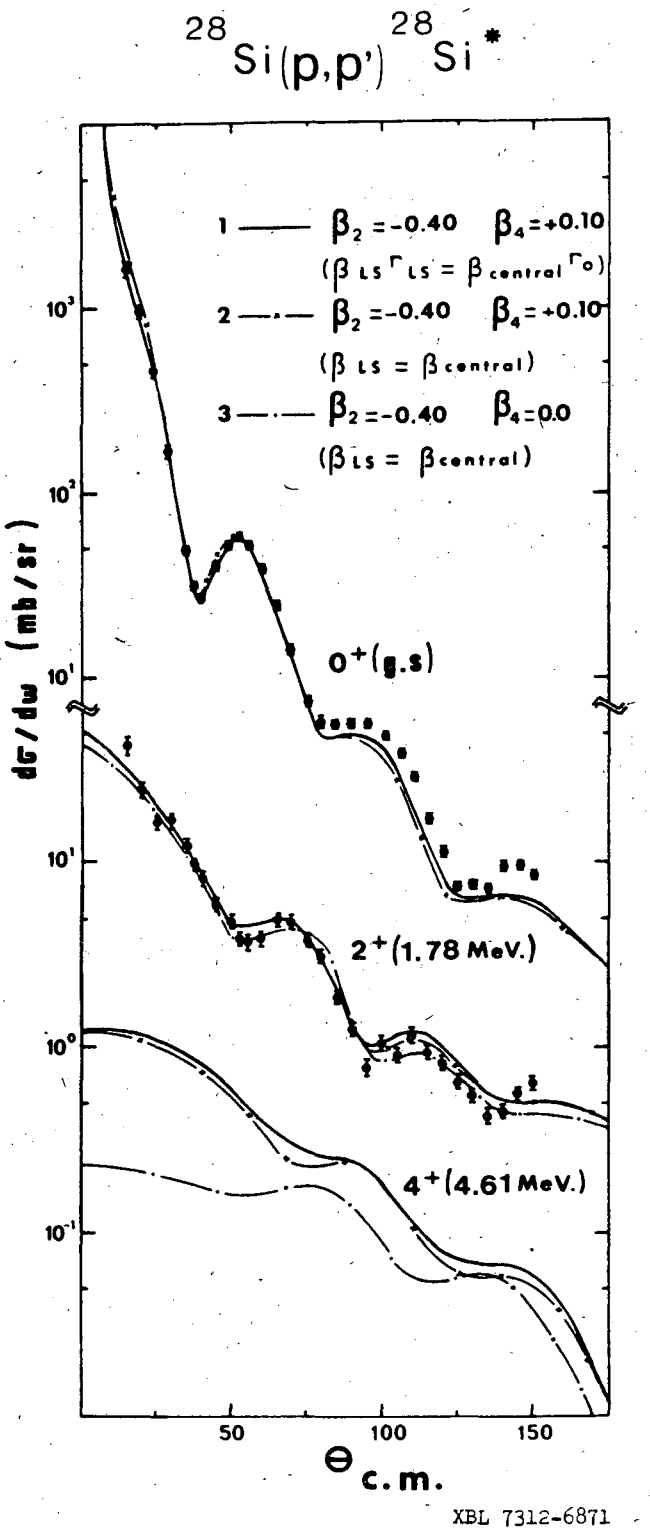
$^{28}Si(p,p')^{28}Si^*$
1 —— $\beta_2 = -0.40$ $\beta_4 = +0.10$
($\beta_{LS} \Gamma_{LS} = \beta_{central} \Gamma_0$)
2 —·— $\beta_2 = -0.40$ $\beta_4 = +0.10$
($\beta_{LS} = \beta_{central}$)
3 —··— $\beta_2 = -0.40$ $\beta_4 = 0.0$
($\beta_{LS} = \beta_{central}$)
0^+(g.s)
2^+(1.78 MeV.)
4^+(4.61 MeV.)
$d\sigma/d\omega$ (mb/sr)
10^3
10^2
10^1
10^1
10^0
10^{-1}
50
100
150
$\Theta_{c.m.}$
XBL 7312-6871

Fig. 13.

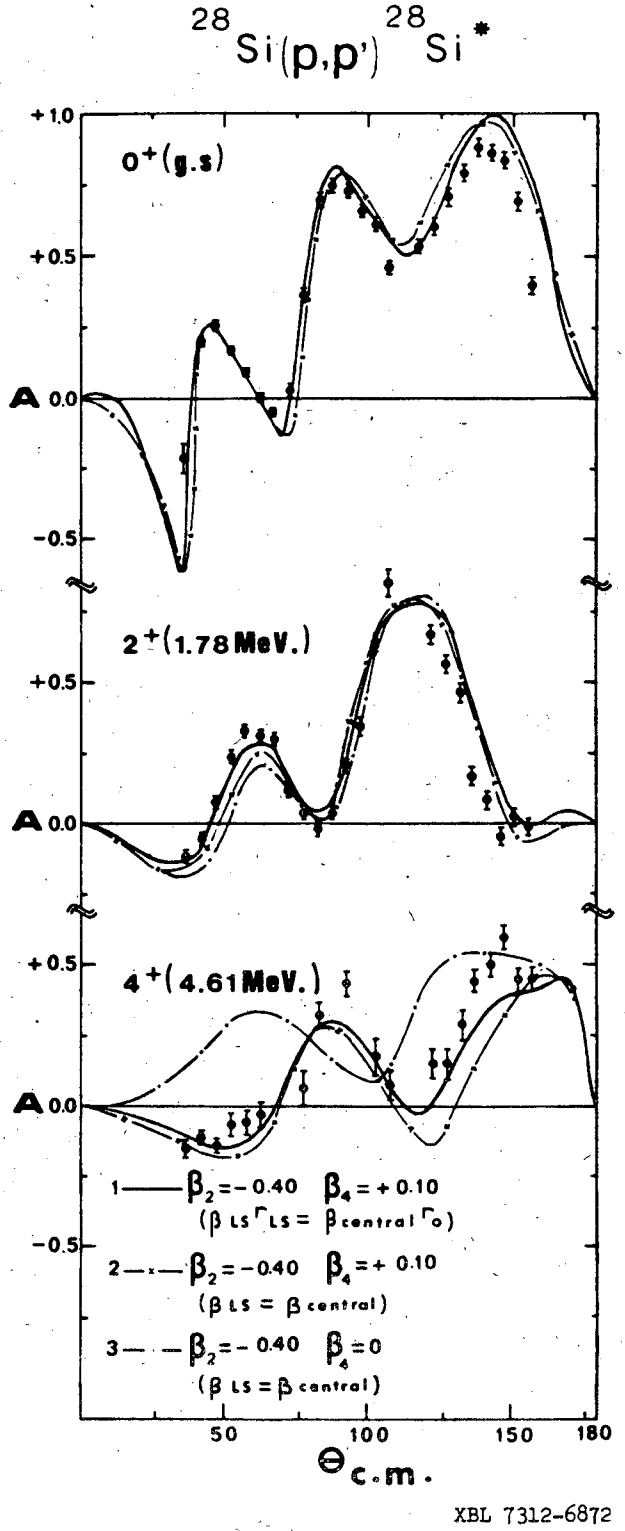
$^{28}Si(p,p')^{28}Si^*$
+1.0
+0.5
A 0.0
-0.5
0^+(g.s)
2^+(1.78 MeV.)
4^+(4.61 MeV.)
1—— $\beta_2 = -0.40$ $\beta_4 = +0.10$
($\beta_{LS}\Gamma_{LS} = \beta_{central}\Gamma_0$)
2—·— $\beta_2 = -0.40$ $\beta_4 = +0.10$
($\beta_{LS} = \beta_{central}$)
3— — $\beta_2 = -0.40$ $\beta_4 = 0$
($\beta_{LS} = \beta_{central}$)
50
100
150
180
$\Theta_{c.m.}$
XBL 7312-6872

Fig. 14.

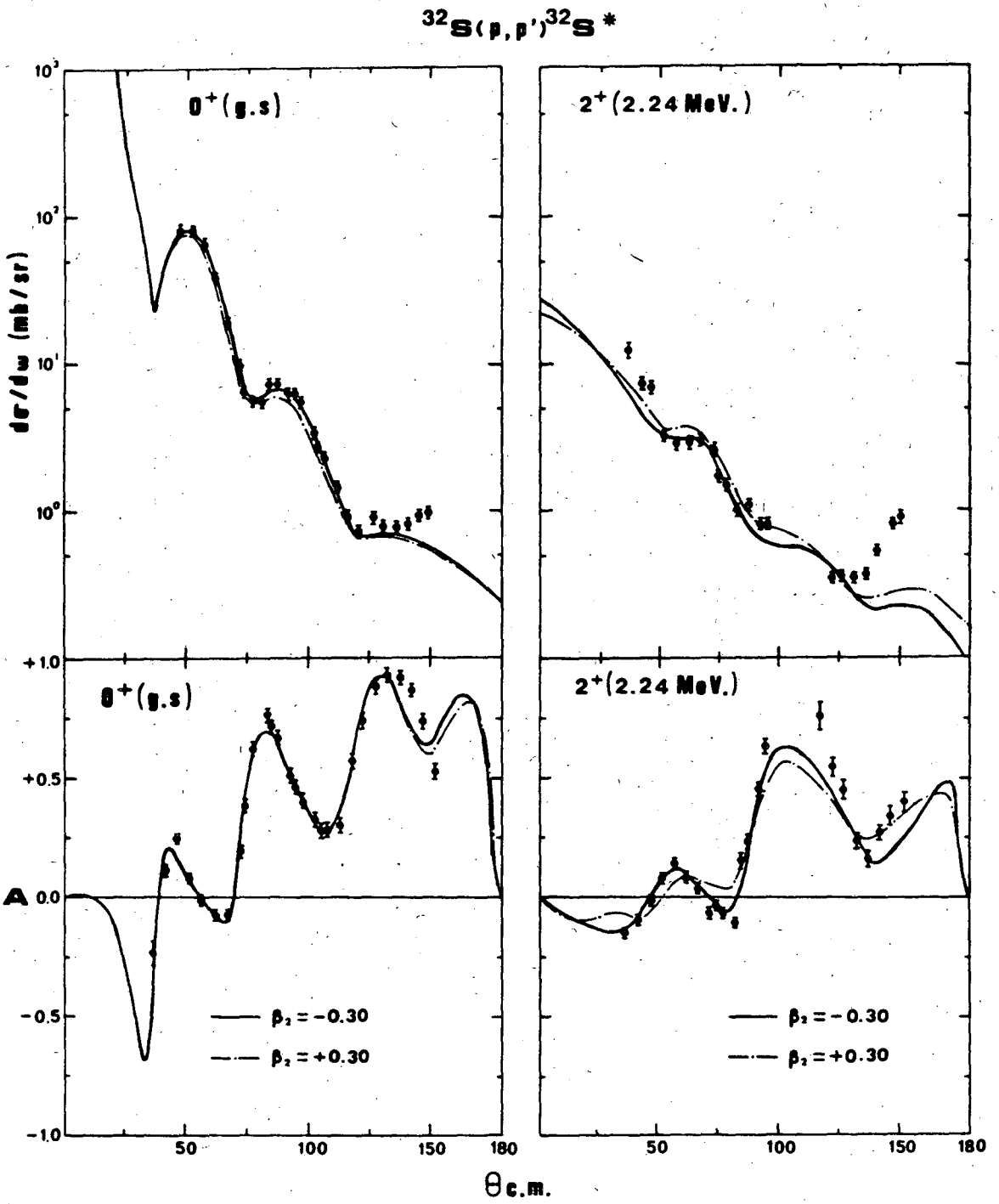
$^{32}S(p,p')^{32}S^*$
0^+(g.s)
2^+(2.24 MeV.)
$d\sigma/d\omega$ (mb/sr)
A
$\beta_2 = -0.30$
$\beta_2 = +0.30$
$\theta_{c.m.}$
XBL 7312-6873

Fig. 15.

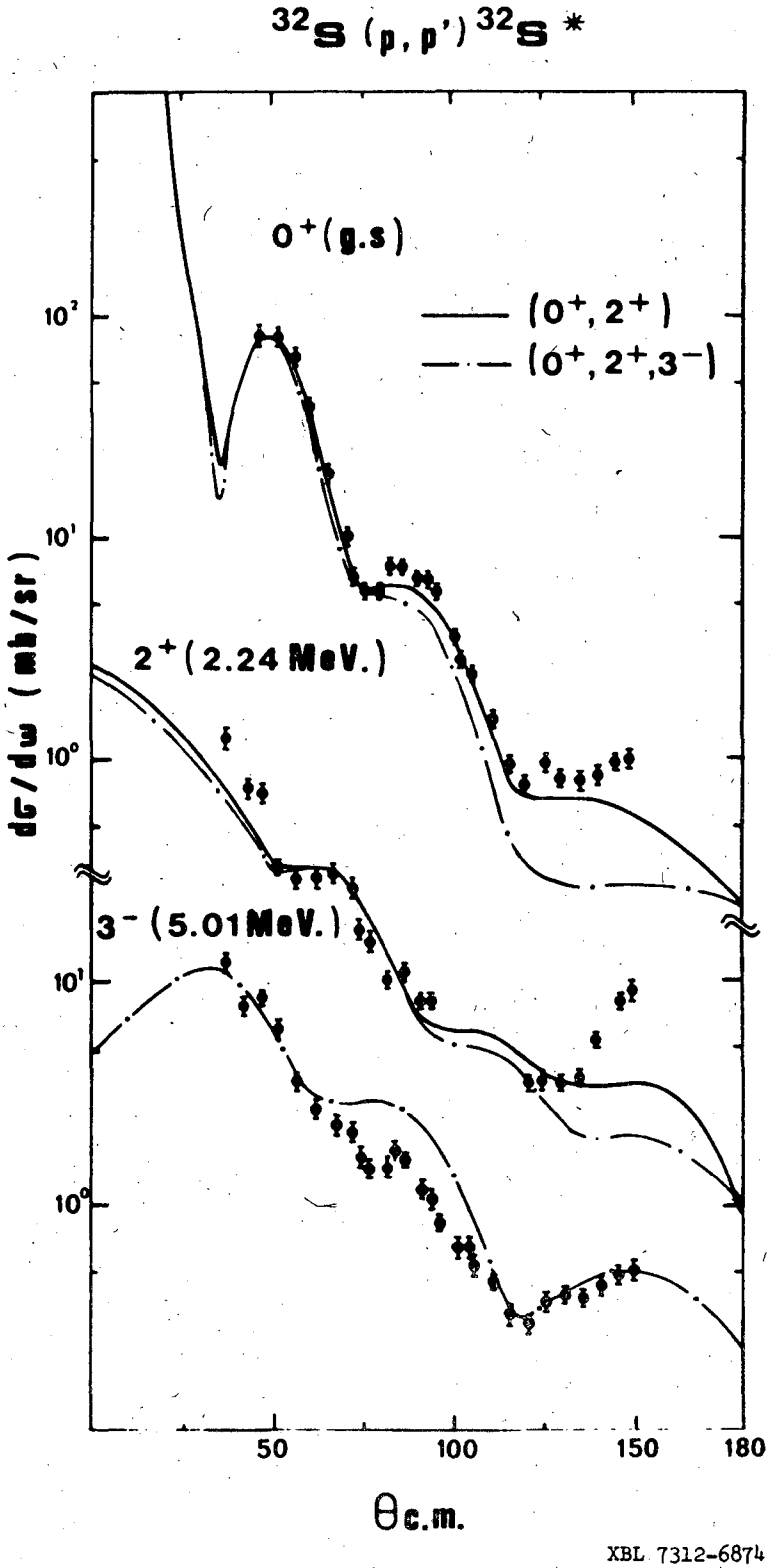
$^{32}S\ (p, p')\ ^{32}S^*$
0^+(g.s)
$(0^+, 2^+)$
$(0^+, 2^+, 3^-)$
2^+(2.24 MeV.)
3^-(5.01MeV.)
10^2
10^1
10^0
10^1
10^0
dσ/dω (mb/sr)
50
100
150
180
θc.m.
XBL 7312-6874

Fig. 16.

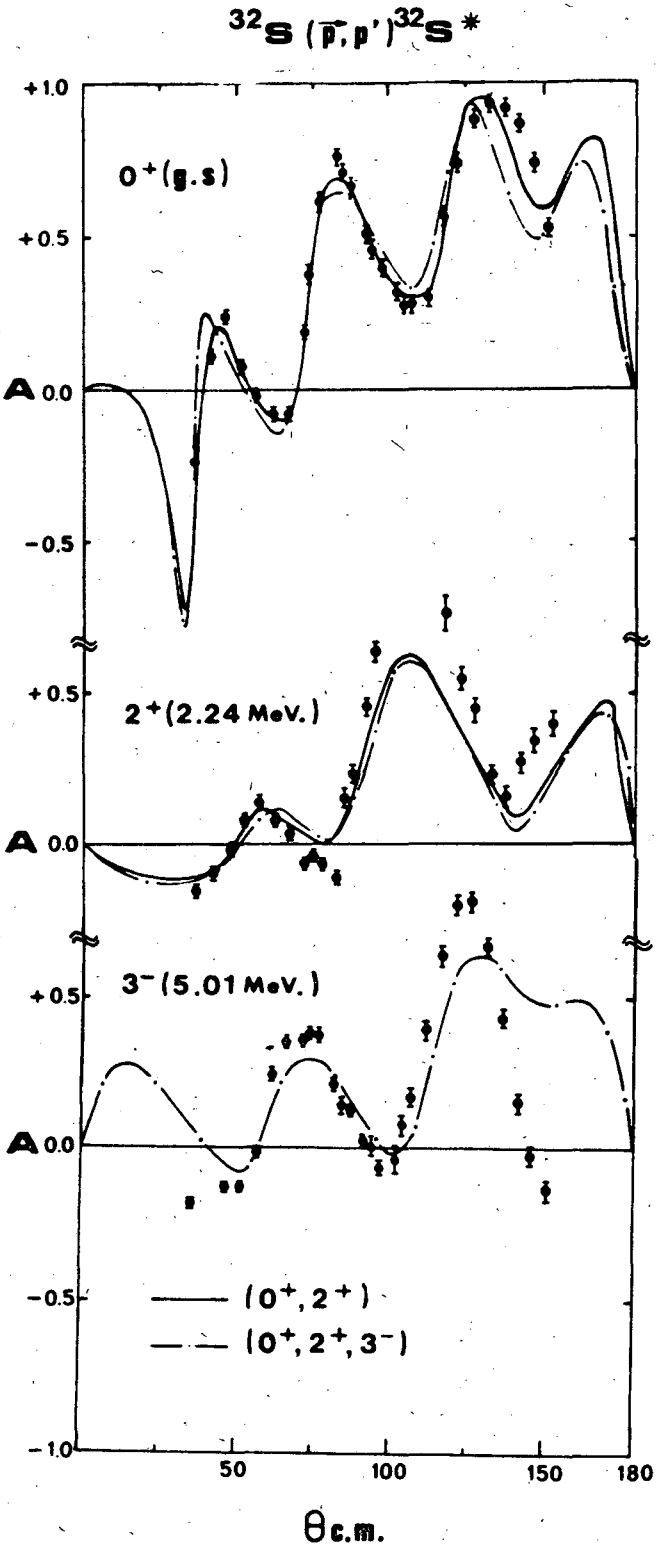
$^{32}S(\vec{p},p')^{32}S^*$
0^+(g.s)
2^+(2.24 MeV.)
3^-(5.01 MeV.)
A
+1.0
+0.5
0.0
-0.5
-1.0
50
100
150
180
$(0^+, 2^+)$
$(0^+, 2^+, 3^-)$
$\theta_{c.m.}$
XBL 7312-6875

Fig. 17.

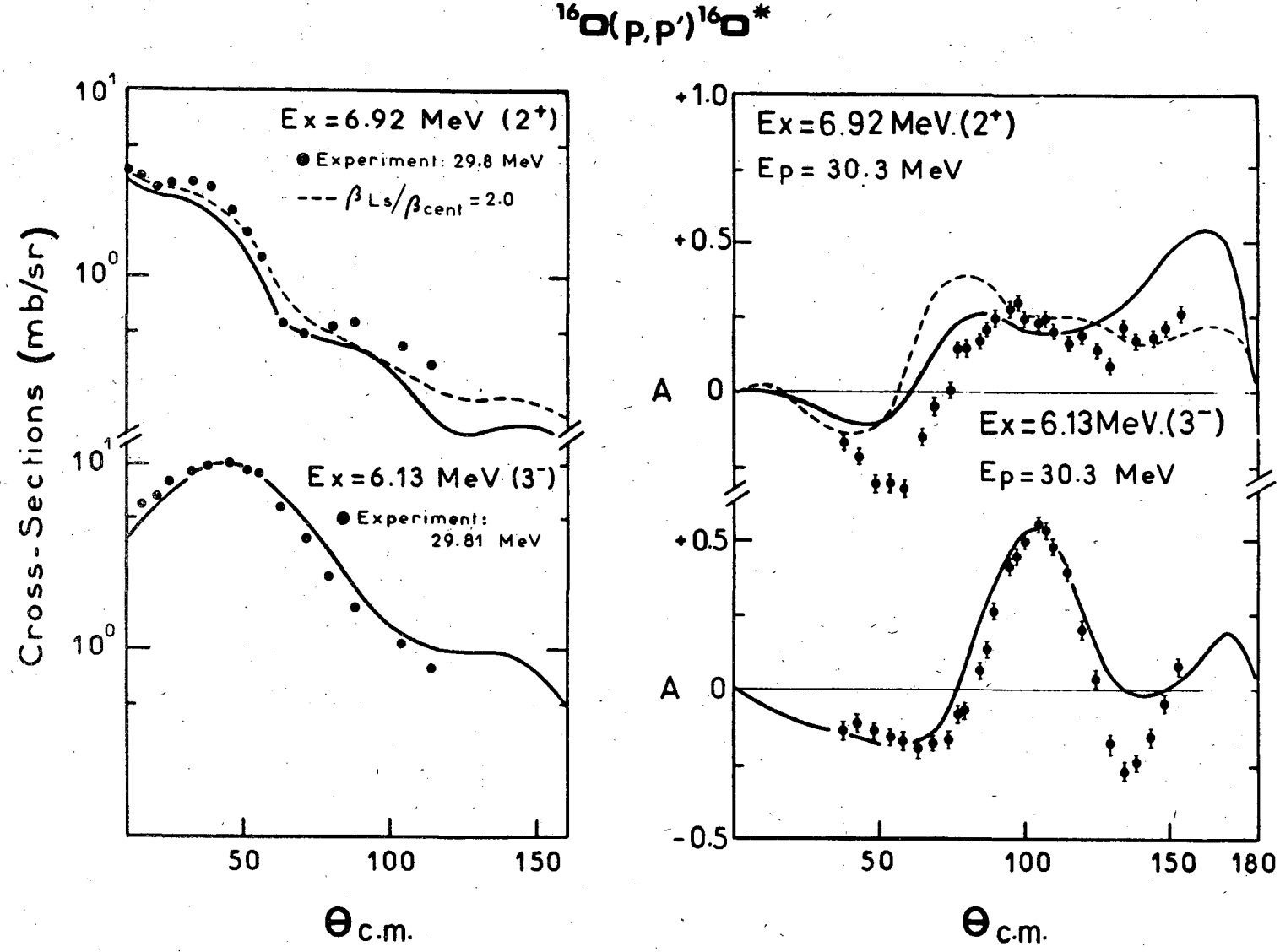

XBL 7312-6876

Fig. 18.

TECHNICAL INFORMATION DIVISION
LAWRENCE BERKELEY LABORATORY
UNIVERSITY OF CALIFORNIA
BERKELEY, CALIFORNIA 94720